

Response to Editor – Round 2

Thanks for your detailed responses and revisions. The manuscript is accepted, but please do make one more very minor change before you submit the final version. Please put line 64-67 back to your introduction, since it is important to mention that.

Thanks for the input – you're correct in that these lines are important. They have been added back into the revised manuscript.

1 **Convective distribution of dust over the Arabian Peninsula: the** 2 **impact of model resolution**

3 Jennie Bukowski¹, Susan C. van den Heever¹

4 ¹ Department of Atmospheric Science, Colorado State University, Fort Collins, CO

5 *Correspondence to:* Jennie Bukowski (jennie.bukowski@colostate.edu)

6 **Abstract**

7 Along the coasts of the Arabian Peninsula, convective dust storms are a considerable source of mineral dust to the
8 atmosphere. Reliable predictions of convective dust events are necessary to determine their effects on air quality,
9 visibility, and the radiation budget. In this study, the Weather Research and Forecasting Model coupled with
10 Chemistry (WRF-Chem) is used to simulate a 2016 summertime dust event over the Arabian Peninsula and examine
11 the variability in dust fields and associated vertical transport due to the choice of convective parameterization and
12 convection-allowing versus parameterized convection. Simulations are run at 45 km and 15 km grid spacing with
13 multiple cumulus parameterizations, and are compared to a 3 km simulation that permits explicit dry and moist
14 convective processes. Five separate cumulus parameterizations at 15 km grid spacing were tested to quantify the
15 spread across different parameterizations. Finally, the impact these variations have on radiation, specifically aerosol
16 heating rates is also investigated.

17 On average, in these simulations the convection-permitting case produces higher quantities of dust than the
18 parameterized cases in terms of dust uplift potential, vertical dust concentrations, and vertical dust fluxes. Major
19 drivers of this discrepancy between the simulations stem from the convection-allowing case exhibiting higher
20 surface windspeeds during convective activity, lower dust emission wind threshold velocities due to drier soil, and
21 more frequent, stronger vertical velocities which transport dust aloft and increase the atmospheric lifetime of these
22 particles. For aerosol heating rates in the lowest levels, the shortwave effect prevails in the convection-permitting
23 case with a net cooling effect, whereas a longwave net warming effect is present in the parameterized cases. The
24 spread in dust concentrations across cumulus parameterizations at the same grid resolution (15 km) is an order of
25 magnitude lower than the impact of moving from parameterized towards explicit convection. We conclude that
26 tuning dust emissions in coarse resolution simulations can only improve the results to first-order and cannot fully
27 rectify the discrepancies originating from disparities in the representation of convective dust transport.

28 **1) Introduction**

29 Airborne mineral dust is an important atmospheric aerosol (Zender et al., 2004; Ginoux et al., 2012): dust reduces
30 visibility (e.g. Mahowald et al., 2007; Baddock et al., 2014; Camino et al., 2015) and is detrimental to the human
31 respiratory system (Prospero, 1999; van Donkelaar et al., 2010; Stafoggia et al., 2016), but also plays a vital role in

32 fertilizing iron-deficient maritime ecosystems (Martin, 1991; Bishop et al., 2002; Mahowald et al., 2005; Jickells
33 and Moore, 2015). Dust particles function as cloud condensation nuclei (e.g. Lee et al., 2009; Manktelow et al.,
34 2009; Twohy et al., 2009; Karydis et al., 2011) and ice nuclei (e.g. DeMott et al., 2003; Field et al., 2006; Knopf and
35 Koop, 2006; Boose et al., 2016), thereby altering cloud development and properties. Furthermore, mineral dust is of
36 interest due to its distinctive optical properties; dust both scatters and absorbs shortwave and longwave radiation
37 (e.g. Tegen et al., 1996; Kinne et al., 2003; Dubovik et al., 2006) modifying atmospheric thermodynamics and the
38 earth's energy budget in the process (e.g. Slingo et al., 2006; Sokolik and Toon, 2006; Heald et al., 2014).

39 The influence of atmospheric mineral dust is widespread in the weather and climate system, yet generating skillful
40 forecasts of dust concentrations and their temporal and spatial evolution has been difficult to achieve. Several
41 studies suggest that including the radiative effects of mineral dust in numerical weather prediction (NWP) could
42 refine the radiation balance of these models and improve forecasts (Kischa et al., 2003; Haywood et al., 2005; Pérez
43 et al., 2006). Advances in climate models have been made by incorporating time-varying dust sources and climate-
44 dust feedbacks in the radiative forcing calculations (Kok et al., 2014; Woodage and Woodward, 2014; Kok et al.,
45 2018). However, these potential improvements are contingent upon the quality of the dust model and initialization
46 data, which models are known to be especially sensitive to. As such, substantial discrepancies exist across global
47 models of similar resolution (Huneus et al., 2011), and across regional models (Uno et al., 2006; Todd et al., 2008)
48 in the magnitude of predicted dust flux from the surface to the atmosphere.

49 A major challenge in modeling dust processes is the scales of motion involved in its emission and subsequent
50 transport. Dust particles mobilize from the surface due to wind erosion of arid soils, a mechanism that occurs on the
51 micron scale, but once airborne mineral dust can deposit locally or be transported on the synoptic to global scales.
52 Dust events initiate from both large-scale and synoptic dynamical flow regimes, as well as mesoscale features.
53 Synoptic scale uplift phenomena include monsoon troughs (e.g. Marsham et al., 2008), Shamal winds (e.g. Yu et al.,
54 2015) and frontal systems (e.g. Beegum et al. 2018), while dynamical effects on smaller (meso) scales can raise dust
55 through the production of convective outflow boundaries, or haboobs, (e.g. Miller et al. 2008), daytime turbulence
56 or dry convective processes (e.g. Klose and Shao, 2012), and the morning mixing of nocturnal low level jet (NLLJ)
57 momentum to the surface (e.g. Fiedler et al. 2013). When considering only meteorological dust sources, wind drives
58 dust emissions, meaning that the underlying processes that contribute to the wind fields must be resolved in a model
59 to create an accurate dust forecast.

60 One potential source of disagreement in models stems from the scaling emissions in dust parameterizations, which
61 relate the surface emissions proportionally to the second or third power of surface windspeed. This means that minor
62 miscalculations in modeled windspeeds go on to produce more substantial errors in the dust concentration
63 calculations (e.g. Menut, 2008). Current aerosol forecast and climate models are run at fine enough grid-spacing to
64 simulate synoptic events but still typically employ cumulus parameterizations, which are incapable of resolving dry
65 and moist mesoscale updrafts and downdrafts that can potentially loft and / or scavenge dust. Schepanski et al.
66 (2015) found that online dust models are likely to be most sensitive to the initialization data compared to other

67 model options, which adds additional uncertainty to dust forecasts. Pope et al. (2016) and Largeron et al. (2015)
68 both postulated that an inadequate representation of convection in coarse model simulations, specifically the
69 underestimation of high surface windspeeds in mesoscale haboobs, is a major contributor to errors in dust models.
70

71 The misrepresentation of dust concentrations in models with cumulus parameterizations has been investigated across
72 several modeling platforms, mostly from the perspective of dust lofting mechanisms at the surface. Heinold et al.
73 (2013) ran the UK Met Office Unified Model (UM) over West Africa with offline dust emissions, and found that of
74 the factors they tested, the model was most sensitive to explicit versus parameterized convection. Furthermore, in
75 the Heinold et al. (2013) study, dust emissions were reduced as grid resolution was increased to convection-
76 permitting scales by roughly 50%. This was found to be due to the parameterized simulations underestimating moist
77 convective activity but drastically overestimating the NLLJ dust uplift mechanism, a similar relationship to that
78 originally identified in Marsham et al. (2011).

79 Conversely, studies using different numerical dust models have identified other relationships between horizontal
80 resolution and dust emissions. Roberts et al. 2018 also used UM to investigate this relationship over the Sahara and
81 Sahel and reported little change in the dust emissions when moving from parameterized to explicit convection, but
82 also noted that the NLLJ maximum decreased as the convective maximum increased. Reinfried et al. (2009)
83 simulated a haboob case study from Morocco with the Lokal Modell - MultiScale chemistry aerosol transport (LM-
84 MUSCAT, since renamed COSMO-MUSCAT) regional model and found increased dust emissions in a convection-
85 allowing simulation versus those with cumulus parameterizations. They also established that the model was more
86 sensitive to the choice of cumulus parameterization rather than the change in horizontal resolution. Similarly, Bouet
87 et al. (2012) identified an increase in dust emissions with increasing model resolution using the Regional
88 Atmospheric Modeling System coupled to the Dust Prediction Model (RAMS-DPM) while simulating a Bodélé
89 depression case study. Ridley et al. (2013) showed that global aerosol models with parameterized convection were
90 also sensitive to model resolution and that higher horizontal resolution led to higher dust emissions.
91

92 With the added computational expense of running aerosol code, the resolution of dust forecast models lags relative
93 to their weather-only prediction counterparts for both global and regional prediction systems (Benedetti et al., 2014;
94 Benedetti et al., 2018). Global dust forecasts generated by several aerosol models are available through the Sand and
95 Dust Storm Warning Advisory and Assessment System (SDS-WAS) (<http://www.wmo.int/sdswas>), but none
96 of the models in the SDS-WAS are currently run at fine enough grid-spacing to be considered convection-permitting
97 (SDS-WAS Model inter-comparison and forecast evaluation technical manual; last updated January, 2018). While
98 regional numerical weather prediction models have moved into convection-permitting scales, the added
99 computational cost of aerosol parameterizations means that convective parameterizations will be a necessity for
100 longer in models that employ online aerosol predictions. It is also clear that horizontal model resolution remains an
101 understudied factor in regional dust modeling. As such, exploring differences across cumulus parameterizations and
102 those relative to convection-permitting resolutions continues to be relevant and vital to better understand aerosol
103 forecasting and aerosol-cloud-environment interactions.

104 While previous studies have begun to examine the effect of horizontal model resolution on dust emissions and
105 airborne dust concentrations, there are several factors that warrant more investigation. As it stands, there is little
106 agreement on the sign of the response in dust emissions to a change in horizontal model resolution, which seems to
107 vary based on the regional model being utilized. Most studies have concentrated on the change in dust emissions
108 based on moving from parameterized convection to convection-allowing scales, while ignoring the possible
109 sensitivity due to the choice of the cumulus parameterization itself. Furthermore, much of the previous literature
110 focused on how the increase in resolution affects convective outflow boundaries and surface / near-surface processes
111 as dust sources, rather than convective transport and the vertical redistribution of dust and its radiative effects at
112 different levels of the atmosphere. In this paper, we seek to address these limitations in the understanding of the
113 effects of horizontal model resolution on dust concentrations. The goal of the research presented here is therefore to
114 quantify the sign and magnitude in the response of modeled dust fields in a regional numerical model to increasing
115 horizontal resolution.

116 In order to achieve our stated goal, we will use numerical simulations of a case study to examine the variability in
117 dust emissions and vertical dust concentrations and fluxes due to (1) the choice of convective parameterization, (2)
118 convection-allowing versus parameterized convection, and (3) the impact of these variations on radiation,
119 specifically aerosol heating rates. These simulations are performed using the Weather Research and Forecasting
120 Model coupled with Atmospheric Chemistry (WRF-Chem) (Skamarock et al., 2008; Grell et al., 2005; Fast et al.,
121 2006) a platform that has been tested for its sensitivity to vertical resolution for dust extinction coefficient profiles
122 (Teixeira et al., 2015) and horizontal model resolution and convective transport for chemical species such as carbon
123 monoxide (e.g. Klich and Fuelberg, 2013), but not for dust. These simulations will represent a case study of a
124 summertime coastal convective dust event over the Arabian Peninsula, a relatively understudied region compared to
125 areas such as the Sahara (Jish Prakash et al., 2015), despite being the world's second largest dust emission region
126 (Tanaka and Chiba, 2004).

127 This paper is part of a larger body of collaborative work conducted by the Holistic Analysis of Aerosols in Littoral
128 Environments (HAALE) research team under the Office of Naval Research Multidisciplinary Research Program of
129 the University Research Initiative (MURI). The primary goal of the HAALE-MURI project is to isolate the
130 fundamental environmental factors that govern the spatial distribution and optical properties of littoral zone aerosols.
131 The study discussed in this manuscript focuses on advancing our understanding in the role that convection plays in
132 the redistribution of dust aerosol and its radiative effects along the coast of arid regions, and seeks to quantify the
133 uncertainty in forecasted dust distributions stemming from the representation of convective processes in a regional
134 model.

135 The manuscript is organized as follows: an overview of the WRF-Chem model and physics setup (Sect. 2.1), dust
136 model setup (Sect. 2.2), information about the cumulus parameterizations and model resolution (Sect. 2.3), and
137 analysis methods in Sect. 2.4. A description of the case study is found in Sect. 2.5. The results are outlined in Sect.
138 3, with a discussion on the temporal evolution of dust concentrations and dust uplift potential in Sect. 3.1, vertical

139 distributions and fluxes of dust in Sect. 3.2, and the effect on aerosol radiative heating rates in Sect. 3.3. A
140 discussion of the results and implications for the community are located in Sect. 4 and a summary of the findings of
141 this study are reviewed in Sect. 5.

142 **2) Case study and model description**

143 **2.1) WRF-Chem model description and physics**

144 To investigate the Arabian Peninsula case study, WRF-Chem version 3.9.1.1 was used to simulate the dust outbreak
145 meteorology and aerosol fields. WRF-Chem is an online numerical chemical transport model that allows for
146 interactive aerosol processes, including feedbacks between the meteorology, aerosol, and radiation. The model was
147 coupled to the Goddard Chemistry Aerosol Radiation and Transport (GOCART) module (Ginoux et al., 2001),
148 which allowed for feedbacks between the meteorology and aerosols and is described in more detail in Sect. 2.2. The
149 model was tested with and without dust initial and boundary conditions from the Community Atmosphere Model
150 with Chemistry (CAM-Chem) global model (Emmons et al. 2010). The concentrations of dust advected through the
151 lateral boundary conditions was too small to have an effect on the results, and the initial conditions introduced a
152 spurious decreasing integrated dust trend over time when modeled aerosol optical depth (AOD) was compared to
153 AERONET observations. While the initial conditions led to a higher integrated dust mass, it did not change the
154 conclusions of the study. To remove this factor and focus more on the meteorological processes that actively loft and
155 transport dust in real-time, no chemistry or aerosol initial / lateral boundary conditions were used. Rather, the
156 aerosol fields were initialized with zero concentrations and were allowed to evolve naturally from the model
157 meteorology, aerosol, surface and radiation processes.

158
159 The meteorological and sea surface temperature initial and lateral boundary conditions were sourced from the 0.25
160 degree, 6-hourly Global Data Assimilation System Final Analysis (GDAS-FNL). The model was run from 00:00:00
161 UTC on 02-Aug-2016 to 00:00:00 UTC on 05-Aug-2016 producing output at 30-minute intervals. The following
162 model parameterizations were employed and kept constant across the simulations, with similar WRF physics options
163 being utilized elsewhere to study dust effects (e.g. Alizadeh Choobari et al. 2013): Morrison double-moment
164 microphysics (Morrison et al., 2005; 2009), RRTMG longwave scheme (Iacano et al., 2008), Goddard shortwave
165 radiation scheme (Chou and Suarez, 1999), the Noah Land Surface Model with multiparameterization options (Niu
166 et al., 2011; Yang et al., 2011), and the MYNN level 3 boundary layer parameterization (Nakanishi and Niino, 2006;
167 2009). The convective parameterizations and horizontal resolutions tested will be discussed in Sect. 2.4. A summary
168 of the physics options utilized can be found in Table 1.

169

170 **2.2) GOCART dust emissions and dust uplift potential**

171 WRF-Chem is coupled to the GOCART dust module, which parameterizes the emission of dry mineral dust mass
172 from the surface. GOCART is single-moment in mass, meaning there is no number information available to change

173 the number of cloud condensation nuclei or ice nuclei in the microphysics. As such, the indirect effects of dust
 174 cannot be simulated with this setup. Through this model, dust is emitted to the atmosphere in 5 discrete effective
 175 radii bins [0.5, 1.4, 2.4, 4.5, and 8.0 μm] based on Eq. (1):

$$176 \quad F_p = CSs_p U^2(U - U_t) \text{ if } U > U_t \quad (1)$$

177 In Eq. (1), F_p is the dust flux from the surface [$\text{kg m}^{-2} \text{s}^{-1}$] for each of the radii bins (p), S represents the wind erosion
 178 scaling factor [0 to 1] established by the Ginoux et al. (2004) soil erodibility map, s_p is the fraction of each size class
 179 within the soil [0 to 1] based on the silt and clay fraction of the soil type, U is the 10 m wind speed [m s^{-1}], and U_t is
 180 the threshold velocity of wind erosion [m s^{-1}]. C is a tuning constant (set here to a default $1 \text{ kg s}^2 \text{ m}^{-5}$), which can be
 181 set by the user to increase or decrease the total dust flux based on regional observations (e.g. Zhao et al., 2010;
 182 Kalenderski et al., 2013; Dipu et al., 2013). If the wind speed is less than the threshold velocity, no dust will loft
 183 from the surface. Most of the terms in Eq. (1) are time invariant (C, S, s_p), except for the wind speed (U) and wind
 184 erosion threshold (U_t). U_t is a function of soil wetness, and is calculated with the relationship found in Eq. (2):

$$185 \quad U_t = \begin{cases} 6.5 \sqrt{\frac{\rho_p - \rho_a}{\rho_a}} g D_p (1.2 + \log_{10} w_{soil}) & \text{if } w_{soil} < 0.5 \\ \infty & \text{if } w_{soil} \geq 0.5 \end{cases} \quad (2)$$

186 For Eq. (2), ρ_p is the dust particle density [kg m^{-3}], ρ_a is the density of air [kg m^{-3}], g is gravitational acceleration [m
 187 s^{-2}], and w_{soil} is the soil wetness fraction [0 to 1]. Similar to Eq. (1), Eq. (2) includes a threshold, whereby above a
 188 soil wetness of 0.5, no dust will be emitted. If the threshold criteria are met and dust lofts from the surface, it is then
 189 transported based on the simulated meteorological fields from WRF, including advection, convection, and turbulent
 190 mixing, and is removed from the atmosphere via gravitational settling and wet deposition. Here, wet deposition is
 191 included as a scavenging mechanism to provide a more realistic picture of the moist convection transport process.
 192 Aerosol radiation interactions in the shortwave and longwave (Barnard et al., 2010) are included in the simulations
 193 to understand the implications that lofted dust has on the energy budget of the case study and are discussed in Sect.
 194 3.3.

195 Before dust can amass in and influence the atmosphere, it must first be emitted from the surface. Because of the
 196 threshold values included in the GOCART dust parameterization equations (Eq. 1-2), it is important to understand
 197 how often the modeled near-surface wind speeds exceed the wind threshold value. A parameter useful in describing
 198 the influence of the wind on dust emissions is Dust Uplift Potential (DUP), proposed by Marsham et al. (2011) and
 199 based on Marticorena and Bergametti (1995). The DUP parameter is an offline approximation for the relative
 200 amount of dust expected to loft from the surface. DUP is a convenient way to perform first order sensitivity tests on
 201 the meteorology without having to re-run the model, and provides a framework for deconvolving the variables in Eq.
 202 (1-2). Here, we have adapted the DUP parameter from Marsham et al. (2011) (Eq. 4) into three variations (Eq. 3-5),
 203 which allows researchers to vary the complexity of the analysis by including more, or fewer degrees of freedom.

$$204 \quad DUP(U) = U^3 \left(1 + \frac{A}{U}\right) \left(1 - \frac{A^2}{U^2}\right) \quad (3)$$

205 $DUP(U, U_t) = U^3 \left(1 + \frac{U_t}{U}\right) \left(1 - \frac{U_t^2}{U^2}\right)$ (4)

206 $DUP(U, U_t, S) = SU^3 \left(1 + \frac{U_t}{U}\right) \left(1 - \frac{U_t^2}{U^2}\right)$ (5)

207 In Eq. (3), U_t is set to a constant wind speed, A , thereby making DUP a function of only the near-surface wind
 208 speed; for the purpose of this paper U_t is set to 5 m s^{-1} , but has been tested elsewhere across the range of $5\text{-}10 \text{ m s}^{-1}$
 209 (e.g. Marsham et al., 2011; Cowie et al., 2015; Pantillon et al., 2015). This simplified equation for dust uplift has
 210 been used in previous dust studies, and is useful to include here to place this manuscript in the context of existing
 211 literature. Eq. (4) is slightly more intricate in that it considers the model evolution of U_t due to changing soil wetness
 212 from precipitation and land-surface processes, calculated by Eq. (2). Lastly, Eq. (5) builds on Eq. (4) by including
 213 the soil erodibility scaling factor (S), which recognizes that the U and U_t relationship is valid only if it occurs over
 214 potential dust source regions. Since U , U_t , and S are entangled in the GOCART dust parametrization found in Eq.
 215 (1-2), the seemingly minor variations between the DUP parameters in Eq. (3-5) are crucial for isolating which
 216 processes, or combination of processes, are sensitive to the horizontal resolution of the model, and hence to the
 217 analysis performed here.

218 **2.3) Domain, nesting, and cumulus parameterizations**

219 Several horizontal model grid-spacings (45 km, 15 km, and 3 km) of the Arabian Peninsula domain (Fig. 3) were
 220 tested to identify the sensitivity of modeled dust concentrations to the model's horizontal resolution. For the two
 221 coarsest simulations (45 km and 15 km), cumulus parameterizations were employed to represent shallow and deep
 222 convection. The 45 km simulation was run with only the Betts–Miller–Janjic (BMJ) cumulus parameterization
 223 (Janjic, 1994), while five different cumulus parameterizations were tested for the 15 km simulations, including the
 224 BMJ, Kain–Fritsch (KF) (Kain, 2004), Grell 3D Ensemble (GD) (Grell, 1993; Grell et al., 2002), Tiedtke (TD)
 225 (Tiedtke, 1989; Zhang et al., 2011), and Simplified Arakawa–Schubert (AS) (Arakawa and Schubert, 1974; Han and
 226 Pan, 2011) schemes, which will determine the sensitivity of dust lofting to different cumulus parameterizations. A
 227 15 km simulation with no cumulus parameterization was also run, but the results were similar and within the spread
 228 of the 15 km simulations that employed cumulus parameterizations and are not included here. The finest resolution
 229 simulation (3 km) was run at convection-permitting scales and hence no cumulus parameterizations were invoked.
 230 The 3 km simulation was initialized as a one-way nest from the 15 km BMJ simulation, which served as its parent
 231 lateral boundary conditions. Other combinations of nests were tested, but the results were not sensitive to which 15
 232 km simulation was used as the parent nest, or lateral boundary conditions, for the 3 km simulation. A summary of
 233 the model domains is also found in Fig. 3.

234 The cumulus parameterizations tested in this study for the 15 km simulations vary in their methods for triggering
 235 and then characterizing convective processes at the sub-grid scale level. BMJ is a moisture and temperature
 236 adjustment scheme that acts to restore the pre-convective unstable thermodynamic profile to a post-convective stable
 237 and well-mixed reference profile, while the other cumulus parameterizations (KF, GD, TD, AS) employ a mass-flux
 238 approach to determine updraft and downdraft mass transport. Across the mass-flux parameterizations, GD is unique

239 in that it computes an ensemble of varying convective triggers and closure assumptions and then feeds the ensemble
240 mean back to the model. Furthermore, all five schemes represent shallow convection in addition to deep convection,
241 the mass-flux schemes include detrainment of water and ice at cloud top, and AS and TD are formulated to include
242 momentum transport in their calculations. These differences across parameterizations will result in varying updraft
243 and downdraft speeds and precipitation rates, which will have consequences for the vertical transport of airborne
244 dust, as well as the strength of convective outflow boundaries and therefore dust emission at the surface. Several
245 cumulus parameterization schemes were tested to introduce spread into the solutions and to represent the 15 km
246 results as a 5-member ensemble mean with uncertainty estimates. Because this paper seeks to investigate the effect
247 of horizontal resolution on dust transport, comparing individual cumulus schemes against one another is outside the
248 scope of this study.

249 **2.4) Averaging and analysis methods**

250 Because the representation of convective processes varies across the simulations, the results will focus on composite
251 statistics from the three-day case study. The authors make no attempt to track and match individual convective
252 elements across simulations, as their triggering, timing, and development (or lack of development) will fluctuate
253 depending on the model resolution and cumulus parameterization, thus making a truly consistent analysis
254 problematic. Instead, this paper takes a step backward and aims to quantify in an average sense, how the choice of
255 horizontal resolution and parameterized convection affects dust concentrations in the WRF-Chem model across the
256 Arabian Peninsula. The analyses and averages are processed within the yellow box shown in Fig. 3, disregarding all
257 other grid points outside the Arabian Peninsula study area. Analyses that are averaged in time are only averaged
258 over the last two days of the simulation (00:00:00 UTC on 03-Aug-2016 to 00:00:00 UTC on 05-Aug-2016) to
259 account for model spin up in the first 24 hours. All results are summed over the five dust bins in the GOCART
260 model rather than being treated separately. Lastly, the results from the five 15 km simulations are averaged together
261 to produce a mean 15 km resolution response, and is presented, along with the maximum and minimum spread
262 across these simulations for reference.

263 **2.5) Case study overview**

264 The dust event simulated for this study occurred during August 2-5, 2016 across the Arabian Peninsula, originating
265 from a combination of synoptic and mesoscale dust sources. A meteorological analysis of this event, including an
266 attribution of specific dust sources to meteorological features can be found in Miller et al. (2019) and will not be
267 reiterated in detail here. Rather, a snapshot of the meteorology and dust fields from the WRF-Chem simulation on
268 August 3rd at 15:00:00 UTC can be found in Fig. 1-2 as a reference to the typical meteorological setup for this case
269 study.

270 For this event, the high summertime temperatures in the desert of the Arabian Peninsula produce a thermal low
271 couplet at the surface, with one low centered over Iraq and the other over the Rub' al Khali desert in Saudi Arabia
272 (Fig. 1.c). The local low-pressure couplet leads to cyclonic surface winds between these two areas (Fig. 1.e),
273 comprised of northerly flow from Iraq into Saudi Arabia, with retuning southerly flow from Oman over the Persian

274 Gulf and into Kuwait, and is a major non-convective contributor to the dust budget for this case study (Fig. 1.f). In
275 addition to these large-scale flow patterns, a daytime sea breeze brings moist, maritime air from the coast of Yemen
276 and Oman inland into the otherwise arid Saudi Arabian basin (Fig. 1.e and 1.d). This moisture gradient is also
277 evident in the skew-t diagrams, which represent an inland radiosonde release site at Riyadh (Fig. 2.a), and a site
278 closer to the coast in Abha (Fig. 2.b), both located in Saudi Arabia. There is a stark difference in low-level moisture
279 between the two sites, although both display a subsidence inversion aloft between 500 and 600 hPa. Furthermore,
280 nocturnal low-level jets form along the Zagros mountains in Iran and Iraq, and the Red sea, both of which have been
281 studied previously in the literature (Giannakopoulou and Toumi, 2011; Kalenderski and Stenchikov, 2016).

282 Due to the region's inherent moisture constraints, convection is limited spatially to the coastal regions of the
283 Arabian Peninsula, as is most summertime convective and non-convective precipitation in this region (e.g. Shwehdi,
284 2005; Almazroui, 2011; Hasanean and Almazroui, 2015; Babu et al., 2016). Moist convective cells develop along a
285 low-level convergence line between the northerly basin flow and sea breeze front (Fig. 1.g and 1.h) aided by
286 elevated terrain in Yemen and Oman (Fig. 1.a). This convective setup along the southern portion of the Arabian
287 Peninsula is a feature evident in each day of this case study, initializing diurnally in the local late afternoon and early
288 evening, and thereby providing three days of data for analysis, with the height of convective activity occurring on
289 August 3rd. Individual convective cells form along the convergence line, a typical Middle Eastern characteristic
290 (Dayan et al., 2001), but do not organize further, owing to a lack of upper-level synoptic support and insufficient
291 moisture in the interior of the peninsula. Nevertheless, the convective line does produce outflow boundaries, which
292 loft dust from the surface and are the main convective dust source for this case study. More information on model
293 validation of this study, including comparisons of these simulations with AOD observations can be found in Saleeby
294 et al. (2019), which shows that WRF-Chem systematically underestimates dust AOD for this event.

295 **3) Results**

296 **3.1) Temporal evolution**

297 **3.1.1) Dust uplift potential**

298 The first process of interest in determining the sensitivity of modeled dust concentrations to horizontal resolution in
299 WRF-Chem is the amount of dust lofted from the surface to the atmosphere. Fig. 4 depicts the average DUP for the
300 simulations at each 30-minute output, using Eq. (3-5) to separate out the importance of the different mechanisms
301 regulating dust emissions.

302 Regardless of which DUP parameter is used, almost all of the simulations capture the bimodal daily maximum in
303 dust emissions in the local mid-morning (6 UTC) and late afternoon (13 UTC) due to the mixing of the NLLJ to the
304 surface and convective outflow boundaries, respectively. The only resolution where the bimodality is absent is the
305 45 km simulation, which captures the NLLJ mechanism, but misses the second convective activity maximum. The
306 coarsest simulation overestimates the near-surface wind speeds related to the NLLJ mechanism, which subsequently

307 inhibits convection later in the day. Because of this, the 45 km simulation has the highest DUP(U) (Fig. 4.a) based
308 only on wind speed (Eq. 3), a result similar to the Heinhold et al. (2013) and Marsham et al. (2011) studies over the
309 Sahara.

310 However, when taking the calculated threshold wind velocity into account (Eq. 4), the convection-allowing
311 simulation (3 km) displays the strongest DUP(U,U) at the local late afternoon convective maximum (Fig. 4.c). For
312 this to be the case compared to the DUP(U) parameter, the 3 km simulation must have a lower threshold wind
313 velocity (Fig. 5.a) than the simulations with parameterized convection. Since the threshold wind velocity is
314 proportional to soil wetness (Eq. 2), this implies that the convection-permitting simulation will on average have drier
315 soil, or more grid points below the soil wetness threshold than the parameterized simulations. Rainfall is generated
316 differently in parameterized versus convection-allowing simulations, and it has been well documented that
317 parameterized simulations produce more widespread light rainfall, whereas more intense rainfall tends to develop
318 over smaller areas in convection-allowing simulations (e.g. Sun et al., 2006; Stephens et al., 2010). From a domain
319 average perspective, rainfall in the 3 km simulation will cover less area, leading to the soil moisture threshold not
320 being exceeded as frequently compared to the parameterized cases.

321 This spatial difference in rainfall leads to the 3 km case having drier soil on average across the domain, which is
322 evident in the surface fluxes represented by the Bowen ratio of sensible to latent heat fluxes in Fig. 5.c. When the
323 Bowen ratio is above one, more of the surface heat exchange with the atmosphere is in the form of sensible heat
324 flux, rather than latent heat flux. Dry soils are characterized by low values of latent heat flux, and therefore exhibit
325 higher Bowen ratios. The 3 km simulation exhibits a higher Bowen ratio on August 3rd and 4th, indicating that the
326 soil is on average drier in the convection-permitting simulation. This result implies that disparities in land surface
327 properties across the varying model grid resolutions are important for modulating dust emissions, both from the
328 perspective of convection-allowing versus parameterized convection and associated precipitation, as well as latent
329 and sensible heat fluxes.

330 Adding on to the complexity of the DUP parameter, when the location of dust sources is considered in the
331 DUP(U,U_t,S) calculations (Eq. 5), some of variability between the local NLLJ and convection maxima is lost in the
332 3 km simulation (Fig. 4.e) on August 3rd. Also, including the scaling factor reduces the magnitude of the DUP
333 parameter to roughly 10% of the initial values for DUP(U) and DUP(U,U_t). Incorporating the dust source function in
334 DUP works not only as a scaling factor for the magnitude of potential dust emissions, but also impacts the relative
335 importance of dust production mechanisms (NLLJ versus convection). This shift is a consequence of the location in
336 which these processes occur. For instance, the reduction in the 3 km convective maximum on August 3rd between
337 DUP(U,U_t) and DUP(U,U_t,S) signifies that convection is occurring in locations that are not active dust source
338 regions. Without information on the dust source regions, this process would be assigned an unrealistic dominance
339 over the NLLJ mechanism in terms of DUP.

340 All simulations are similar for the first 24 spin-up hours until the processes begin to diverge on August 3rd, where
341 the convection-allowing simulation produces the maximum DUP(U,U_t,S) both during the local daytime and

342 nighttime hours. On the final day of the case study (August 4th), the convection-allowing simulation has the lowest
343 DUP(U,U_t,S), with the NLLJ maximum dominating over the convective maximum in both the 3 km and the 15 km
344 mean, due to reduced convective activity in the fine resolution simulations. Examining the percent difference in
345 DUP between the coarse and fine simulations (Fig. 4.b,d,f), the average percent difference between the 3 km and 15
346 km simulations is at a minimum when only wind speed is considered, and increases as the degrees of freedom in
347 DUP increases. For the DUP(U,U_t,S) case, the average percent difference is between 10-65% lower in the 15 km
348 simulations than the convection-permitting simulation, with a maximum difference of 85% and a spread across
349 parameterizations of 20%. This implies that the convection-allowing WRF-Chem simulation has the potential to loft
350 up to 85% more dust than those with parameterized convection.

351 **3.1.2) Vertically integrated dust mass**

352 The differences in DUP(U,U_t,S), or dust flux from the surface to the atmosphere, specifically the enhanced values
353 for the convection-permitting simulation on August 3rd, will lead to more dust lofting than in the coarse simulations.
354 To see how differences in the dust emissions translate into differences in airborne concentrations of dust, Fig. 6
355 demonstrates the temporal evolution of the spatially averaged, vertically integrated dust mass throughout the vertical
356 column. Here, the convection-allowing simulation records upwards of 150% more integrated dust mass compared to
357 the coarse resolution simulations. Across the coarse simulations, the 45 km and 15 km runs have similar vertically
358 integrated dust magnitudes, despite the temporal differences in DUP(U,U_t,S). This is due to the overestimation of
359 the NLLJ in the 45 km simulations being offset by the enhanced convective dust lofting in the 15 km simulations.

360 The discrepancy in the diurnal maxima across horizontal resolutions is similar to the results of the UM in Marsham
361 et al. (2011) and Heinhold et al. (2013). Yet, the results here differ in that both of these previous studies found a
362 stronger NLLJ response in 12 km simulations with convective parameterizations than was found here in the 15 km
363 parameterized ensemble. In contrast to the findings of Marsham et al. (2011) and Heinhold et al. (2013), dust
364 emissions and airborne dust mass increases in the WRF-Chem simulations in the convection-allowing simulation,
365 which is in closer agreement to the studies of Reinfried et al. (2009) and Bouet et al. (2012) who used COSMO-
366 MUSCAT and RAMS-DPM respectively. Considering each study used a different model and therefore physics, it is
367 unsurprising that the results vary. However, it is not apparent how much of a role the region or specific case study
368 plays in this difference and is an area for future work.

369 The temporal trends in vertically integrated dust mass lag behind those observed in the DUP plots in Fig. 4.
370 Particularly at timesteps where DUP decreases, the change in integrated dust mass follows several hours later. The
371 time series of gravitational settling rates at the surface (Fig. 5.b) also lags behind the DUP trends, which implies that
372 the removal mechanisms for dust take time to act on the airborne particles once they are emitted. The rates of
373 gravitational settling are higher in the convection-permitting simulation compared to the coarse simulations because
374 more dust is available aloft to settle out. Nevertheless, Fig. 6.a suggests that this increase in gravitational settling
375 rates in the 3 km case is not enough to offset the higher dust emissions, or the vertically integrated dust quantities
376 would be similar across all the simulations. The fact that the vertically integrated dust values are higher in the 3 km

377 simulation, despite higher rates of gravitational settling, implies there must be a mechanism that acts to keep dust
378 suspended longer in the convection-permitting simulations than in those with parameterized convection. There are
379 clearly more processes occurring above the surface to influence the vertically integrated dust quantities than just a
380 simple surface emission to surface deposition ratio. This will be further deconstructed by examining vertical profiles
381 in the following section.

382 **3.2) Vertical characteristics**

383 **3.2.1) Vertical dust and velocity profiles**

384 Moving away from vertically integrated quantities to a time and domain averaged vertical snapshot of dust (Fig.
385 7.a), the vertical dust profile follows a generally exponentially decreasing function and tapers off to low dust
386 concentrations in the range of 5-6 km above ground level (AGL). A widespread subsidence inversion is present near
387 6 km throughout the case study time period over the inner basin of the Arabian Peninsula (Fig 2), acting as a cap on
388 vertical motions and dust transport. Because dust concentrations do not vary much above this height, the plots in
389 Fig. 7 have been truncated at 9 km. There is a higher concentration of dust at every level in the convection-allowing
390 simulation compared to that in the coarse simulations. Examining the percent difference plot between the
391 convection-permitting and other simulations in Fig. 7.b, there is a difference of approximately 80% at the surface,
392 which increases upwards to ~180% at 6 km. Above this level, the percent difference between the convection-
393 permitting and coarse simulations changes sign, but the overall concentration is extremely low, and as such, the
394 authors make no attempt to assign meaning to the differences above 6 km.

395 For dust to reach higher levels in the atmosphere, it must have undergone vertical transport to move it aloft from its
396 initial source region at the surface. Several mechanisms could be responsible for vertical dust transport in the
397 Arabian Peninsula, including flow over terrain, daytime mixing (dry convection), and lastly, moist convective
398 updrafts, whose representation (explicit versus parameterized) is a defining difference between the horizontal
399 resolutions tested in this paper. Investigating the effect that increasing resolution has on updraft and downdraft
400 strength can be found in Fig. 8, which represents the mean of all vertical velocities above or below 0 m s^{-1} , including
401 points that are not vertically continuous. As resolution increases, the average range in vertical velocity also
402 increases. The simulations with parametrized convection have lower mean updraft / downdraft speeds than the
403 convection-allowing simulation, on the order ~75% weaker near the surface for the 15 km runs and ~110% weaker
404 for the 45 km run. It is known that in numerical models, the updraft radius scales with the grid spacing (e.g. Bryan
405 and Morrison, 2012), with a compensating increase in updraft speed as the radius decreases. This relationship skews
406 the frequency of vertical velocities to higher values. Irrespective of resolution, the mean updraft speeds in the WRF-
407 Chem simulations are slightly higher than the downdraft speeds, while at the surface mean downdraft speeds are
408 higher than updraft speeds, a consideration that will be discussed further in Sect. 3.2.2.

409 3.2.2) Vertical dust flux

410 The implication for dust transport based on vertical velocities is convoluted, since updrafts and downdrafts work
411 concurrently to redistribute aerosol. As noted in Jung et al. (2005), convective updrafts will lift aerosol particles
412 upward into the free atmosphere, while downdrafts simultaneously limit the maximum vertical extent of these
413 particles. However, the convective transport simulations in Jung et al. (2005) demonstrate that these opposing
414 processes do not act as equal opposites in time, magnitude, and space. This canon holds true for the Arabian
415 Peninsula simulations as well. Fig. 9 contains Contoured Frequency by Altitude Diagrams (CFADs) of vertical
416 velocity (Yuter and Houze, 1995) normalized by the total number of grid points in each simulation. The
417 normalization is performed to remove an artificial larger frequency in the higher resolution simulations that arises
418 because there are more grid spaces available to count. Because no vertical velocity threshold is imposed, a majority
419 of points straddle zero. To highlight variability away from the zero line, the CFAD contours are plotted on a log
420 scale.

421 Similar to the mean plots in Fig. 8, as resolution increases, so does the variability in updraft and downdraft speeds.
422 There is a striking difference between the spread in vertical velocities at all altitudes across the 45 km, 15 km mean,
423 and 3 km simulations in Fig. 9. In the 45 km run, most of the velocities straddle $\pm 1-2 \text{ m s}^{-1}$, whereas the
424 convection-permitting simulation ranges from -10 to 30 m s^{-1} . Not only is the range larger, but the normalized
425 frequency is greater in the fine resolution simulation as well. The inference here is that stronger updrafts will
426 transport dust higher in the atmosphere, and that stronger updrafts are observed more frequently in the convection-
427 allowing simulation, thereby enhancing the vertical dust transport.

428 Combining the information on the vertical distribution of dust and updraft / downdraft speeds, it is possible to
429 calculate a domain averaged dust flux profile (Fig. 8). Again, the magnitude of the dust flux upwards and
430 downwards from the surface through 6 km AGL is higher in the convection-allowing simulation compared to the
431 parametrized simulations. Moreover, the mean near-surface upwards dust flux is stronger than that for the downward
432 dust flux, which coincides with the mean updraft speeds being slightly higher than the mean downdraft speeds at
433 these same vertical levels (Fig. 8). This relationship also holds in the dust flux CFADs (Fig. 9), in which the upward
434 and downward flux of dust has more variability in the 3 km simulation, and stronger vertical dust fluxes are more
435 frequent.

436 Similarly, there is more dust transport evident at higher vertical levels in the convection-permitting simulation,
437 which has implications for the residence time of the dust particles. As dust is transported higher in the atmosphere,
438 absent any sort of external motion or coagulation outside of gravitational settling, the atmospheric lifetime of the
439 particles will increase. Figure 10 shows the theoretical terminal velocity of dust particles in WRF-Chem using the
440 Stokes settling velocity with slip correction for pressure dependence (Fig. 10.a) and their lifetime based on different
441 starting heights in the atmosphere (Fig. 10.b), which increases exponentially away from the surface. As such, dust in
442 the convection-permitting simulation will take longer to settle out, leading to the higher observed vertically
443 integrated dust values (Fig. 5) compared to the parameterized simulations. Looking at the distribution of downdrafts

444 in the vertical velocity CFADs (Fig. 9), there is a clear bimodal signal aloft in both the convection-permitting and 15
445 km simulations, being representative of two distinct subsidence layers, which act as a cap on vertical transport. The
446 local minimum occurs around 6 km, which could explain why dust fluxes also taper off at this level.

447 At the surface, higher dust flux values are found in association with the downdrafts, producing a pronounced
448 skewness towards high, yet infrequent values of strong negative dust flux towards the ground (Fig. 9). It is
449 hypothesized that this skewness is a consequence of the dissimilar background dust conditions in the vicinity of
450 near-surface downdrafts and updrafts, similar to the results found in Siegel and van den Heever (2012), which
451 studied the ingestion of dust by a supercell storm. Updrafts originate in relatively clear air, and will consume
452 background dust and transport it upwards. However, downdrafts occur through the cold pool, and hence their source
453 is, at least partially, within the dusty cold pool. As such, downdrafts will have access to more dust and thus transport
454 more of it in the downward direction. This skewness warrants further research, preferably from an idealized
455 perspective, to better understand the relationship between storm dynamics, dust emissions, and transport.

456 In all, the increased vertical dust concentration profile and vertically integrated dust values in the 3 km run are a
457 product of several processes working together. Compared to the simulations with parameterized convection, the 3
458 km run has enhanced potential for dust uplift due to stronger resolved downdrafts and lower wind velocity
459 thresholds, higher vertical transport due to more frequent, stronger updrafts, and a lengthier theoretical residence
460 time once being lofted to higher levels.

461 **3.3) Impacts on radiation**

462 Beyond the first-order sensitivity of model resolution to dust emissions and concentrations for the Arabian Peninsula
463 case study, there are higher-order effects that disseminate from changing dust concentrations. One example being
464 the modification of atmospheric heating / cooling rates and the radiation budget due to dust absorption and scattering
465 (see Sect. 1). The domain and time averaged shortwave (SW), longwave (LW), and net dust heating / cooling rates
466 are found in Fig. 11. The average dust heating and cooling rates were calculated over the last 48 hours of the
467 simulation as a difference between the radiation tendency with dust aerosols and without. Ostensibly, since dust
468 concentrations increase in the model as resolution increases, so does the magnitude of the radiative effects. There is
469 a stronger SW cooling and LW heating effect in the 3 km simulation, and this trend follows the vertical distribution
470 of dust from Fig. 7, again tapering off near 5-6 km AGL.

471 Most interestingly, however, is the difference in the net aerosol heating rate. In the lowest layer (<1.5 km), there is a
472 sign change between the fine and coarse simulations. The SW effect in the convection-allowing simulation is strong
473 enough to elicit a net cooling effect in this near-surface layer. Conversely, the LW aerosol heating effect dominates
474 in the coarse simulations, resulting in a net warming effect. The model has a stronger shortwave effect for dust based
475 on the prescribed index of refraction, but is also related to the timing of dust emissions, considering the SW effect is
476 only active during the daytime. The difference between warming and cooling can have cascading effects on the
477 thermodynamic profile, static stability, and future convective development, which in turn impacts the relative

478 importance between convection and the NLLJ discussed earlier. The sensitivity of dust concentrations to horizontal
479 model resolution is important to understand in its own right, but furthermore, this sensitivity leads to higher-order
480 changes in model predictions. If NWP models or GCMs are going to incorporate dust radiative effects,
481 concentrations need to be highly constrained, not only to accurately capture the magnitude, but the sign of the
482 response as well.

483 **4) Discussion and recommendations**

484 For this Arabian Peninsula event, horizontal resolution in the WRF-Chem model has a considerable effect on the
485 dust budget of the region. Because aerosol prediction models and GCMs still employ cumulus parameterizations, it
486 is important to discuss the uncertainties unearthed in this paper, as well as recommendations for past and future
487 forecasts and research that will be generated prior to our ability to consistently run these models at convection-
488 permitting resolutions.

489 In an average sense, there will be higher dust concentrations produced in convection-permitting simulations
490 compared to those with parameterized convection. The major point here is that the uncertainty in dust concentrations
491 for simulations using different cumulus parameterizations (15 km ensemble), or using different horizontal
492 resolutions with the same cumulus parameterizations (45 km versus 15 km) is small relative to the differences
493 between the use of parameterized versus convection-allowing scales. *Most of the uncertainty in the model's*
494 *predicted dust concentrations comes from the choice to either parameterize convection or run at convection-*
495 *permitting scales.*

496 The results of this research do not stand alone in the literature focused on the impact of horizontal model resolution
497 on dust emissions, and there are several similarities and differences to note when comparing this paper to previous
498 studies. Firstly, concerning the diurnal variation in dust emissions, we find a similar response in the NLLJ
499 mechanism to that of Heinhold et al. (2013) and Marsham et al. (2011), whereby the coarsest simulations
500 overestimate the early morning windspeeds caused by the mixing of the jet to the surface and fail to capture the late
501 afternoon / early evening convective dust lofting mechanism. In these previous studies, the convection-allowing
502 simulation reduces the importance of the NLLJ and enhances the convective maximum, but still retains the NLLJ as
503 the dominant process for dust uplift. Overall, Heinhold et al. (2013) and Marsham et al. (2011) found a net reduction
504 in dust uplift while running at convection-permitting scales. While the NLLJ mechanism is found to be similar here,
505 the analysis reveals an opposite response in WRF-Chem for the Arabian Peninsula, in which the convective
506 maximum dominates, but the NLLJ is still an important mechanism, which thereby leads to more, rather than less
507 dust in the convection-allowing simulations. The net increase in dust concentrations in WRF-Chem is similar to the
508 findings of Reinfried et al. (2009), although Reinfried et al. (2009) focused mainly on haboobs, which may point to
509 convection being the source of agreement rather than the balance between the NLLJ and convection. At this point,
510 we cannot determine whether the discrepancies between our results and previous literature comes from regional or
511 case study differences in the importance of these mechanisms to the dust budget, differences in the models'

512 representation of these processes, or a combination of the two. In all, more work needs to be done to investigate the
513 relationship between the NLLJ and subsequent late afternoon convection in dust producing regions, and the
514 representation of this in numerical models.

515 From a vertically integrated viewpoint, for the Arabian Peninsula region it is possible to rudimentarily tune the dust
516 concentrations of the coarse simulations to that of the convection-permitting simulation by multiplying by an
517 average constant derived from the dust difference plots in Fig. 6-7, which would be on the order of ~ 2 . This is an
518 offline solution, which would aid in enhancing the accuracy of a first-order forecast of vertically integrated or
519 surface dust, and/or AOD. This factor would have to be scaled further, since comparison of the WRF-Chem model
520 to AERONET sites and other AOD observations (Saleeby et al. 2019) shows that WRF-Chem underestimates dust
521 under these conditions. Nevertheless, attempting to use this tuning parameter online in the model (i.e. adjusting the
522 tuning constant, C , in Eq. 1) would not reconcile the differences from a dust flux standpoint. Even if more dust were
523 to be emitted from the surface, the parameterized simulations still lack the necessary variability in updrafts and
524 downdrafts, especially updraft strength, to transport the dust upwards and away from the surface, thus
525 misrepresenting the atmospheric lifetime of these particles in the process.

526 Moreover, tuning the dust concentrations will not change the effect horizontal resolution has on the soil
527 characteristics, particularly soil moisture, and hence on the a priori determined threshold wind speeds which are
528 important in calculating dust lofting in the first place (Fig. 4). If dust concentrations are inaccurately predicted in the
529 coarse simulations, or erroneously tuned, the higher-order online feedbacks will also be incorrect, such as
530 modifications to the radiative budget, and feedbacks to the thermodynamic profile, static stability and mesoscale
531 features, particularly those driven by differences in thermodynamic gradients, such as sea breezes and cold pool
532 propagation.

533 **5) Conclusions**

534 In this study, we have quantified the response sign and magnitude in modeled dust fields in the WRF-Chem regional
535 model to increasing horizontal resolution and the manner in which convection is represented for a summertime
536 Arabian Peninsula event. We have investigated the variability in dust concentrations and fluxes due to the choice of
537 convective parameterization, the representation of convection in the model (explicit versus parameterized), and the
538 effect these differences in dust concentrations have on aerosol heating rates. The case study was simulated at three
539 different horizontal resolutions (45 km, 15 km, and 3 km), with the two coarsest simulations run with cumulus
540 parameterizations, and the 3 km simulation run at convection-permitting resolution. To understand the uncertainty
541 across different parameterizations, five separate cumulus parameterizations were tested in an ensemble (BMJ, AS,
542 GD, TD, KF) at 15 km grid spacing.

543 The convection-allowing simulation exhibited a stronger potential for dust uplift as a function of modeled wind
544 speed, wind threshold, and the location of dust sources. The wind threshold for dust lofting in the 3 km simulation
545 was on average, lower than that for the 15 km or 45 km. This is due to differences in grid resolution leading to

546 changes in the soil moisture, whereby the 3 km simulation displays lower soil wetness across the domain.
547 Furthermore, a distinct difference across simulations was identified in the representation of the bimodal daily
548 maximum in dust emissions in the local mid-morning (mixing of the NLLJ to the surface) and late afternoon
549 (convective outflow boundaries). Compared to the 3 km case, the 45 km simulation overestimates the contribution
550 from the NLLJ and underestimates the role of convection in dust emissions.

551 The 3 km simulation also produced higher vertically integrated dust values at every timestep, as well as higher dust
552 concentrations at every vertical level in the lower troposphere (below 6 km AGL). The uncertainty in dust
553 concentrations for simulations using different cumulus parameterizations (15 km ensemble spread) is much smaller
554 than the difference between the parameterized and convection-permitting convection cases. For the WRF-Chem
555 Arabian Peninsula simulations, the modeled dust fields were most sensitive to the choice of parametrizing or
556 explicitly resolving convective processes. The enhanced dust concentrations in the convection-allowing case are the
557 result of stronger downdrafts lofting more dust from the surface, and stronger updrafts carrying dust to higher levels
558 of the atmosphere, thereby increasing the airborne lifetime of the dust particles. The difference in dust mass across
559 the simulations leads to a significant modification of the radiation budget, specifically the aerosol heating rate. The
560 convection-allowing simulation revealed a greater shortwave and longwave effect, and for aerosol heating rates in
561 the lowest levels, shortwave cooling is stronger than longwave heating, leading to a net cooling effect. Conversely,
562 the opposite radiative response is present in the parameterized cases, resulting in a net warming effect, causing a
563 change in sign in the lowest levels compared to the convection-permitting case.

564 There are a number of implications these results may have on forecasting and future studies. The dust concentrations
565 in the coarse simulations could be tuned offline to match those in the convection-allowing simulation using the
566 percentage difference plots included in Fig. 5-6. This tuning would be on the order of ~ 2 . However, because vertical
567 transport is essential to the vertical concentrations and lifetime of the particles, this tuning factor cannot be applied
568 online. Even if such a tuning were applied, this change will not accurately capture higher-order feedbacks to the
569 meteorology, thermodynamic environment and radiation budget of the Arabian Peninsula, or to the soil moisture
570 wind threshold velocities. Finally, this work also points to the need to better constrain dust concentrations in
571 numerical models, and further develop our understanding of the relationship between storm dynamics and dust
572 processes.

573 **Author contributions**

574 Jennie Bukowski (JB) and Susan C. van den Heever (SvdH) designed the experiments. JB set up and performed the
575 WRF-Chem simulations and wrote the analysis code. Both JB and SvdH contributed to the analysis of the model
576 output. JB prepared the manuscript with contributions and edits from SvdH.

577 **Competing interests**

578 The authors declare that they have no conflict of interest.

579 **Acknowledgements**

580 This work was funded by an Office of Naval Research – Multidisciplinary University Research Initiative (ONR-
581 MURI) grant (# N00014-16-1-2040). Jennie Bukowski was partially supported by the Cooperative Institute for
582 Research in the Atmosphere (CIRA) Program of Research and Scholarly Excellence (PRSE) fellowship. The
583 simulation data are available upon request from the corresponding author, Jennie Bukowski. Initialization data for
584 the model was provided by: National Centers for Environmental Prediction, National Weather Service, NOAA, U.S.
585 Department of Commerce. 2000, updated daily. NCEP FNL Operational Model Global Tropospheric Analyses,
586 continuing from July 1999. Research Data Archive at the National Center for Atmospheric Research, Computational
587 and Informational Systems Laboratory. <https://doi.org/10.5065/D6M043C6>.

588 **References**

- 589 Alizadeh Choobari, O., Zawar-Reza, P., and Sturman, A.: Low level jet intensification by mineral dust aerosols,
590 *Ann. Geophys.*, 31, 625–632, doi:10.5194/angeo-31-625-2013, 2013.
- 591 Almazroui, M.: Calibration of TRMM rainfall climatology over Saudi Arabia during 1998–2009, *Atmos. Res.*,
592 99(3–4), 400–414, doi:10.1016/J.ATMOSRES.2010.11.006, 2011.
- 593 Aoki, T., Tanaka, T. Y., Uchiyama, A., Chiba, M., Mikami, M., Yabuki, S. And Key, J. R.: Sensitivity Experiments
594 of Direct Radiative Forcing Caused by Mineral Dust Simulated with a Chemical Transport Model, *J.*
595 *Meteorol. Soc. Japan. Ser. II*, 83A, 315–331, doi:10.2151/jmsj.83A.315, 2005.
- 596 Arakawa, A. and Schubert, W. H.: Interaction of a Cumulus Cloud Ensemble with the Large-Scale Environment,
597 Part I, *J. Atmos. Sci.*, 31(3), 674–701, doi:10.1175/1520-0469(1974)031<0674:IOACCE>2.0.CO;2, 1974.
- 598 Babu, C. A., Jayakrishnan, P. R. and Varikoden, H.: Characteristics of precipitation pattern in the Arabian Peninsula
599 and its variability associated with ENSO, *Arab. J. Geosci.*, 9(3), 186, doi:10.1007/s12517-015-2265-x,
600 2016.
- 601 Baddock, M. C., Strong, C. L., Leys, J. F., Heidenreich, S. K., Tews, E. K. and McTainsh, G. H.: A visibility and
602 total suspended dust relationship, *Atmos. Environ.*, 89, 329–336, doi:10.1016/J.ATMOSENV.2014.02.038,
603 2014.
- 604 Barnard, J. C., Fast, J. D., Paredes-Miranda, G., Arnott, W. P. and Laskin, A.: Technical Note: Evaluation of the
605 WRF-Chem “Aerosol Chemical to Aerosol Optical Properties Module” using data from the MILAGRO
606 campaign, *Atmos. Chem. Phys.*, 10(15), 7325–7340, doi:10.5194/acp-10-7325-2010, 2010.
- 607 Beegum, S. N., Gherboudj, I., Chaouch, N., Temimi, M. and Ghedira, H.: Simulation and analysis of synoptic scale
608 dust storms over the Arabian Peninsula, *Atmos. Res.*, 199, 62–81, doi:10.1016/J.ATMOSRES.2017.09.003,
609 2018.
- 610 Benedetti, A., Reid, J. S., Knippertz, P., Marsham, J. H., Di Giuseppe, F., Rémy, S., Basart, S., Boucher, O., Brooks,
611 I. M., Menut, L., Mona, L., Laj, P., Pappalardo, G., Wiedensohler, A., Baklanov, A., Brooks, M., Colarco,
612 P. R., Cuevas, E., da Silva, A., Escribano, J., Flemming, J., Huneeus, N., Jorba, O., Kazadzis, S., Kinne, S.,
613 Popp, T., Quinn, P. K., Sekiyama, T. T., Tanaka, T. and Terradellas, E.: Status and future of numerical

614 atmospheric aerosol prediction with a focus on data requirements, *Atmos. Chem. Phys.*, 18(14), 10615–
615 10643, doi:10.5194/acp-18-10615-2018, 2018.

616 Benedetti, A., Baldasano, J. M., Basart, S., Benincasa, F., Boucher, O., Brooks, M. E., Chen, J.-P., Colarco, P. R.,
617 Gong, S., Huneeus, N., Jones, L., Lu, S., Menut, L., Morcrette, J.-J., Mulcahy, J., Nickovic, S., Pérez
618 García-Pando, C., Reid, J. S., Sekiyama, T. T., Tanaka, T. Y., Terradellas, E., Westphal, D. L., Zhang, X.-
619 Y. and Zhou, C.-H.: Operational Dust Prediction, in *Mineral Dust: A Key Player in the Earth System*,
620 edited by P. Knippertz and J.-B. W. Stuut, pp. 223–265, Springer Netherlands, Dordrecht., 2014.

621 Benedetti, A., Reid, J. S. and Colarco, P. R.: International Cooperative for Aerosol Prediction Workshop on Aerosol
622 Forecast Verification, *Bull. Am. Meteorol. Soc.*, 92(11), ES48-ES53, doi:10.1175/BAMS-D-11-00105.1,
623 2011.

624 Bishop, J. K. B., Davis, R. E. and Sherman, J. T.: Robotic Observations of Dust Storm Enhancement of Carbon
625 Biomass in the North Pacific, *Science* (80-.), 298(5594), 817 LP-821, doi:10.1126/science.1074961, 2002.

626 Boose, Y., Welti, A., Atkinson, J., Ramelli, F., Danielczok, A., Bingemer, H. G., Plötze, M., Sierau, B., Kanji, Z. A.
627 and Lohmann, U.: Heterogeneous ice nucleation on dust particles sourced from nine~deserts worldwide --
628 Part 1: Immersion freezing, *Atmos. Chem. Phys.*, 16(23), 15075–15095, doi:10.5194/acp-16-15075-2016,
629 2016.

630 Bouet, C., Cautenet, G., Bergametti, G., Marticorena, B., Todd, M. C. and Washington, R.: Sensitivity of desert dust
631 emissions to model horizontal grid spacing during the Bodélé Dust Experiment 2005, *Atmos. Environ.*, 50,
632 377–380, doi:10.1016/J.ATMOSENV.2011.12.037, 2012.

633 Bryan, G. H., and Morrison, H.: Sensitivity of a Simulated Squall Line to Horizontal Resolution and
634 Parameterization of Microphysics, *MWR*, 140, 202-225, doi:10.1175/MWR-D-11-00046.1, 2012.

635 Camino, C., Cuevas, E., Basart, S., Alonso-Pérez, S., Baldasano, J. M., Terradellas, E., Marticorena, B., Rodríguez,
636 S. and Berjón, A.: An empirical equation to estimate mineral dust concentrations from visibility
637 observations in Northern Africa, *Aeolian Res.*, 16, 55–68, doi:10.1016/J.AEOLIA.2014.11.002, 2015.

638 Chou, M.-D. and Suarez, M. J.: Technical Report Series on Global Modeling and Data Assimilation A Thermal
639 Infrared Radiation Parameterization for Atmospheric Studies Revised May 2003, *Nasa Tech. Memo.* 15,
640 NASA, 40 pp., 1999.

641 Corr, C. A., Ziemba, L. D., Scheuer, E., Anderson, B. E., Beyersdorf, A. J., Chen, G., Crosbie, E., Moore, R. H.,
642 Shook, M., Thornhill, K. L., Winstead, E., Lawson, R. P., Barth, M. C., Schroeder, J. R., Blake, D. R. and
643 Dibb, J. E.: Observational evidence for the convective transport of dust over the Central United States, *J.*
644 *Geophys. Res. Atmos.*, 121(3), 1306–1319, doi:10.1002/2015JD023789, 2016.

645 Cowie, S. M., Marsham, J. H. and Knippertz, P.: The importance of rare, high-wind events for dust uplift in northern
646 Africa, *Geophys. Res. Lett.*, 42(19), 8208–8215, doi:10.1002/2015GL065819, 2015.

647 Dayan, U., Ziv, B., Margalit, A., Morin, E. and Sharon, D.: A severe autumn storm over the middle-east: synoptic
648 and mesoscale convection analysis, *Theor. Appl. Climatol.*, 69(1), 103–122, doi:10.1007/s007040170038,
649 2001.

650 Dipu, S., Prabha, T. V., Pandithurai, G., Dudhia, J., Pfister, G., Rajesh, K. and Goswami, B. N.: Impact of elevated

651 aerosol layer on the cloud macrophysical properties prior to monsoon onset, *Atmos. Environ.*, 70, 454–467,
652 doi:10.1016/J.ATMOSENV.2012.12.036, 2013.

653 Emmons, L. K., Walters, S., Hess, P. G., Lamarque, J.-F., Pfister, G. G., Fillmore, D., Granier, C., Guenther,
654 A., Kinnison, D., Laepple, T., Orlando, J., Tie, X., Tyndall, G., Wiedinmyer, C., Baughcum, S. L., and
655 Kloster, S.: Description and evaluation of the Model for Ozone and Related chemical Tracers, version 4
656 (MOZART-4), *Geosci. Model Dev.*, 3, 43–67, doi.org/10.5194/gmd-3-43-2010, 2010. *We acknowledge use*
657 *of NCAR/ACOM CAM-chem global model output available at [https://www.acom.ucar.edu/cam-chem/cam-](https://www.acom.ucar.edu/cam-chem/cam-chem.shtml)*
658 *[chem.shtml](https://www.acom.ucar.edu/cam-chem/cam-chem.shtml).*

659

660 Fadnavis, S., Semeniuk, K., Pozzoli, L., Schultz, M. G., Ghude, S. D., Das, S. and Kakatkar, R.: Transport of
661 aerosols into the UTLS and their impact on the Asian monsoon region as seen in a global model simulation,
662 *Atmos. Chem. Phys.*, 13(17), 8771–8786, doi:10.5194/acp-13-8771-2013, 2013.

663 Fast, J. D., Gustafson Jr., W. I., Easter, R. C., Zaveri, R. A., Barnard, J. C., Chapman, E. G., Grell, G. A. and
664 Peckham, S. E.: Evolution of ozone, particulates, and aerosol direct radiative forcing in the vicinity of
665 Houston using a fully coupled meteorology-chemistry-aerosol model, *J. Geophys. Res. Atmos.*, 111(D21),
666 doi:10.1029/2005JD006721, 2006.

667 Field, P. R., Möhler, O., Connolly, P., Krämer, M., Cotton, R., Heymsfield, A. J., Saathoff, H. and Schnaiter, M.:
668 Some ice nucleation characteristics of Asian and Saharan desert dust, *Atmos. Chem. Phys.*, 6(10), 2991–
669 3006, doi:10.5194/acp-6-2991-2006, 2006.

670 Giannakopoulou, E. M. and Toumi, R.: The Persian Gulf summertime low-level jet over sloping terrain, *Q. J. R.*
671 *Meteorol. Soc.*, 138(662), 145–157, doi:10.1002/qj.901, 2012.

672 Ginoux, P., Chin, M., Tegen, I., Prospero, J. M., Holben, B., Dubovik, O. and Lin, S.-J.: Sources and distributions of
673 dust aerosols simulated with the GOCART model, *J. Geophys. Res. Atmos.*, 106(D17), 20255–20273,
674 doi:10.1029/2000JD000053, 2001.

675 Ginoux, P., Prospero, J. M., Gill, T. E., Hsu, N. C. and Zhao, M.: Global-scale attribution of anthropogenic and
676 natural dust sources and their emission rates based on MODIS Deep Blue aerosol products, *Rev. Geophys.*,
677 50(3), doi:10.1029/2012RG000388, 2012.

678 Grell, G. A., Peckham, S. E., Schmitz, R., McKeen, S. A., Frost, G., Skamarock, W. C. and Eder, B.: Fully coupled
679 “online” chemistry within the WRF model, *Atmos. Environ.*, 39(37), 6957–6975,
680 doi:10.1016/J.ATMOSENV.2005.04.027, 2005.

681 Hasanean, H., Almazroui, M., Hasanean, H. and Almazroui, M.: Rainfall: Features and Variations over Saudi
682 Arabia, *A Review, Climate*, 3(3), 578–626, doi:10.3390/cli3030578, 2015.

683 Haywood, J. M., Allan, R. P., Culverwell, I., Slingo, T., Milton, S., Edwards, J. and Clerbaux, N.: Can desert dust
684 explain the outgoing longwave radiation anomaly over the Sahara during July 2003?, *J. Geophys. Res.*
685 *Atmos.*, 110(D5), doi:10.1029/2004JD005232, 2005.

686 Heald, C. L., Ridley, D. A., Kroll, J. H., Barrett, S. R. H., Cady-Pereira, K. E., Alvarado, M. J. and Holmes, C. D.:

687 Contrasting the direct radiative effect and direct radiative forcing of aerosols, *Atmos. Chem. Phys.*, 14(11),
688 5513–5527, doi:10.5194/acp-14-5513-2014, 2014.

689 Heinold, B., Knippertz, P., Marsham, J. H., Fiedler, S., Dixon, N. S., Schepanski, K., Laurent, B. and Tegen, I.: The
690 role of deep convection and nocturnal low-level jets for dust emission in summertime West Africa:
691 Estimates from convection-permitting simulations, *J. Geophys. Res. Atmos.*, 118(10), 4385–4400,
692 doi:10.1002/jgrd.50402, 2013.

693 Huneus, N., Schulz, M., Balkanski, Y., Griesfeller, J., Prospero, J., Kinne, S., Bauer, S., Boucher, O., Chin, M.,
694 Dentener, F., Diehl, T., Easter, R., Fillmore, D., Ghan, S., Ginoux, P., Grini, A., Horowitz, L., Koch, D.,
695 Krol, M. C., Landing, W., Liu, X., Mahowald, N., Miller, R., Morcrette, J.-J., Myhre, G., Penner, J.,
696 Perlwitz, J., Stier, P., Takemura, T. and Zender, C. S.: Global dust model intercomparison in AeroCom
697 phase I, *Atmos. Chem. Phys.*, 11(15), 7781–7816, doi:10.5194/acp-11-7781-2011, 2011.

698 Jickells, T. and Moore, C. M.: The Importance of Atmospheric Deposition for Ocean Productivity, *Annu. Rev. Ecol.*
699 *Evol. Syst.*, 46(1), 481–501, doi:10.1146/annurev-ecolsys-112414-054118, 2015.

700 Jish Prakash, P., Stenchikov, G., Kalenderski, S., Osipov, S. and Bangalath, H.: The impact of dust storms on the
701 Arabian Peninsula and the Red Sea, *Atmos. Chem. Phys.*, 15(1), 199–222, doi:10.5194/acp-15-199-2015,
702 2015.

703 Jung, E., Shao, Y. and Sakai, T.: A study on the effects of convective transport on regional-scale Asian dust storms
704 in 2002, *J. Geophys. Res. Atmos.*, 110(D20), doi:10.1029/2005JD005808, 2005.

705 Kain, J. S.: The Kain–Fritsch Convective Parameterization: An Update, *J. Appl. Meteorol.*, 43(1), 170–181,
706 doi:10.1175/1520-0450(2004)043<0170:TKCPAU>2.0.CO;2, 2004.

707 Kalenderski, S., Stenchikov, G. and Zhao, C.: Modeling a typical winter-time dust event over the Arabian Peninsula
708 and the Red Sea, *Atmos. Chem. Phys.*, 13(4), 1999–2014, doi:10.5194/acp-13-1999-2013, 2013.

709 Kalenderski, S. and Stenchikov, G.: High-resolution regional modeling of summertime transport and impact of
710 African dust over the Red Sea and Arabian Peninsula, *J. Geophys. Res. Atmos.*, 121(11), 6435–6458,
711 doi:10.1002/2015JD024480, 2016.

712 Karydis, V. A., Kumar, P., Barahona, D., Sokolik, I. N. and Nenes, A.: On the effect of dust particles on global
713 cloud condensation nuclei and cloud droplet number, *J. Geophys. Res. Atmos.*, 116(D23),
714 doi:10.1029/2011JD016283, 2011.

715 Kinne, S., Lohmann, U., Feichter, J., Schulz, M., Timmreck, C., Ghan, S., Easter, R., Chin, M., Ginoux, P.,
716 Takemura, T., Tegen, I., Koch, D., Herzog, M., Penner, J., Pitari, G., Holben, B., Eck, T., Smirnov, A.,
717 Dubovik, O., Slutsker, I., Tanre, D., Torres, O., Mishchenko, M., Geogdzhayev, I., Chu, D. A. and
718 Kaufman, Y.: Monthly averages of aerosol properties: A global comparison among models, satellite data,
719 and AERONET ground data, *J. Geophys. Res. Atmos.*, 108(D20), doi:10.1029/2001JD001253, 2003.

720 Kishcha, P., Alpert, P., Barkan, J., Kirschner, I. and Machenhauer, B.: Atmospheric response to Saharan dust
721 deduced from ECMWF reanalysis (ERA) temperature increments, *Tellus B Chem. Phys. Meteorol.*, 55(4),
722 901–913, doi:10.3402/tellusb.v55i4.16380, 2011.

723 Klich, C. A. and Fuelberg, H. E.: The role of horizontal model resolution in assessing the transport of CO in a

724 middle latitude cyclone using WRF-Chem, *Atmos. Chem. Phys.*, 14(2), 609–627, doi:10.5194/acp-14-609-
725 2014, 2014.

726 Klose, M. and Shao, Y.: Stochastic parameterization of dust emission and application to convective atmospheric
727 conditions, *Atmos. Chem. Phys.*, 12, 7309–7320, doi:10.5194/acp-12-7309-2012, 2012.

728 Knopf, D. A. and Koop, T.: Heterogeneous nucleation of ice on surrogates of mineral dust, *J. Geophys. Res. Atmos.*,
729 111(D12), doi:10.1029/2005JD006894, 2006.

730 Kok, J. F., Mahowald, N. M., Fratini, G., Gillies, J. A., Ishizuka, M., Leys, J. F., Mikami, M., Park, M.-S., Park, S.-
731 U., Van Pelt, R. S. and Zobeck, T. M.: An improved dust emission model – Part 1: Model description and
732 comparison against measurements, *Atmos. Chem. Phys.*, 14(23), 13023–13041, doi:10.5194/acp-14-13023-
733 2014, 2014.

734 Kok, J. F., Ward, D. S., Mahowald, N. M. and Evan, A. T.: Global and regional importance of the direct dust-
735 climate feedback, *Nat. Commun.*, 9(1), 241, doi:10.1038/s41467-017-02620-y, 2018.

736 Largeron, Y., Guichard, F., Bouniol, D., Couvreux, F., Kergoat, L. and Marticorena, B.: Can we use surface wind
737 fields from meteorological reanalyses for Sahelian dust emission simulations?, *Geophys. Res. Lett.*, 42(7),
738 2490–2499, doi:10.1002/2014GL062938, 2015.

739 Lee, Y. H., Chen, K. and Adams, P. J.: Development of a global model of mineral dust aerosol microphysics,
740 *Atmos. Chem. Phys.*, 9(7), 2441–2458, doi:10.5194/acp-9-2441-2009, 2009.

741 Liao, H. and Seinfeld, J. H.: Radiative forcing by mineral dust aerosols: Sensitivity to key variables, *J. Geophys.*
742 *Res. Atmos.*, 103(D24), 31637–31645, doi:10.1029/1998JD200036, 1998.

743 Mahowald, N. M., Ballantine, J. A., Feddema, J. and Ramankutty, N.: Global trends in visibility: implications for
744 dust sources, *Atmos. Chem. Phys.*, 7(12), 3309–3339, doi:10.5194/acp-7-3309-2007, 2007.

745 Mahowald, N. M., Baker, A. R., Bergametti, G., Brooks, N., Duce, R. A., Jickells, T. D., Kubilay, N., Prospero, J.
746 M. and Tegen, I.: Atmospheric global dust cycle and iron inputs to the ocean, *Global Biogeochem. Cycles*,
747 19(4), doi:10.1029/2004GB002402, 2005.

748 Manktelow, P. T., Carslaw, K. S., Mann, G. W. and Spracklen, D. V.: The impact of dust on sulfate aerosol, CN and
749 CCN during an East Asian dust storm, *Atmos. Chem. Phys.*, 10(2), 365–382, doi:10.5194/acp-10-365-
750 2010, 2010.

751 Marsham, J. H., Parker, D. J., Grams, C. M., Taylor, C. M. and Haywood, J. M.: Uplift of Saharan dust south of the
752 intertropical discontinuity, *J. Geophys. Res. Atmos.*, 113(D21), doi:10.1029/2008JD009844, 2008.

753 Marsham, J. H., Knippertz, P., Dixon, N. S., Parker, D. J. and Lister, G. M. S.: The importance of the representation
754 of deep convection for modeled dust-generating winds over West Africa during summer, *Geophys. Res.*
755 *Lett.*, 38(16), doi:10.1029/2011GL048368, 2011.

756 Marticorena, B. and Bergametti, G.: Modeling the atmospheric dust cycle: 1. Design of a soil-derived dust emission
757 scheme, *J. Geophys. Res. Atmos.*, 100(D8), 16415–16430, doi:10.1029/95JD00690, 1995.

758 Martin, J. H.: Iron still comes from above, *Nature*, 353(6340), 123, doi:10.1038/353123b0, 1991.

759 Menut, L.: Sensitivity of hourly Saharan dust emissions to NCEP and ECMWF modeled wind speed, *J. Geophys.*
760 *Res. Atmos.*, 113(D16), doi:10.1029/2007JD009522, 2008.

761 Miller, S. D., Grasso, L., Bian, Q., Kreidenweis, S., Dostalek, J., Solbrig, J., Bukowski, J., van den Heever, S. C.,
762 Wang, Y., Xu, X., Wang, J., Walker, A., Wu, T.-C., Zupanski, M., Chiu, C., and Reid, J.: *A Tale of Two*
763 *Dust Storms: Analysis of a Complex Dust Event in the Middle East*, Atmos. Meas. Tech. Discuss.,
764 doi:10.5194/amt-2019-82, 2019.

765 Miller, S. D., Kuciauskas, A. P., Liu, M., Ji, Q., Reid, J. S., Breed, D. W., Walker, A. L. and Mandoos, A. Al:
766 Haboob dust storms of the southern Arabian Peninsula, J. Geophys. Res. Atmos., 113(D1),
767 doi:10.1029/2007JD008550, 2008.

768 Morrison, H., Curry, J. A. and Khvorostyanov, V. I.: A New Double-Moment Microphysics Parameterization for
769 Application in Cloud and Climate Models. Part I: Description, J. Atmos. Sci., 62(6), 1665–1677,
770 doi:10.1175/JAS3446.1, 2005.

771 Morrison, H., Thompson, G. and Tatarskii, V.: Impact of Cloud Microphysics on the Development of Trailing
772 Stratiform Precipitation in a Simulated Squall Line: Comparison of One- and Two-Moment Schemes, Mon.
773 Weather Rev., 137(3), 991–1007, doi:10.1175/2008MWR2556.1, 2009.

774 Nakanishi, M. and Niino, H.: An Improved Mellor--Yamada Level-3 Model: Its Numerical Stability and Application
775 to a Regional Prediction of Advection Fog, Boundary-Layer Meteorol., 119(2), 397–407,
776 doi:10.1007/s10546-005-9030-8, 2006.

777 Nakanishi, M. and NIINO, H.: Development of an Improved Turbulence Closure Model for the Atmospheric
778 Boundary Layer, J. Meteorol. Soc. Japan. Ser. II, 87(5), 895–912, doi:10.2151/jmsj.87.895, 2009.

779 National Centers for Environmental Prediction/National Weather Service/NOAA/U.S. Department of Commerce:
780 NCEP GDAS/FNL 0.25 Degree Global Tropospheric Analyses and Forecast Grids, Research Data Archive
781 at the National Center for Atmospheric Research, Computational and Information Systems Laboratory,
782 Boulder, CO, <https://doi.org/10.5065/D65Q4T4Z>, 2015.

783 Niu, G.-Y., Yang, Z.-L., Mitchell, K. E., Chen, F., Ek, M. B., Barlage, M., Kumar, A., Manning, K., Niyogi, D.,
784 Rosero, E., Tewari, M. and Xia, Y.: The community Noah land surface model with multiparameterization
785 options (Noah-MP): 1. Model description and evaluation with local-scale measurements, J. Geophys. Res.
786 Atmos., 116(D12), doi:10.1029/2010JD015139, 2011.

787 Pantillon, F., Knippertz, P., Marsham, J. H. and Birch, C. E.: A Parameterization of Convective Dust Storms for
788 Models with Mass-Flux Convection Schemes, J. Atmos. Sci., 72(6), 2545–2561, doi:10.1175/JAS-D-14-
789 0341.1, 2015.

790 Pantillon, F., Knippertz, P., Marsham, J. H., Panitz, H.-J. and Bischoff-Gauss, I.: Modeling haboob dust storms in
791 large-scale weather and climate models, J. Geophys. Res. Atmos., 121(5), 2090–2109,
792 doi:10.1002/2015JD024349, 2016.

793 Pérez, C., Nickovic, S., Pejanovic, G., Baldasano, J. M. and Özsoy, E.: Interactive dust-radiation modeling: A step
794 to improve weather forecasts, J. Geophys. Res. Atmos., 111(D16), doi:10.1029/2005JD006717, 2006.

795 Pope, R. J., Marsham, J. H., Knippertz, P., Brooks, M. E. and Roberts, A. J.: Identifying errors in dust models from
796 data assimilation, Geophys. Res. Lett., 43(17), 9270–9279, doi:10.1002/2016GL070621, 2016.

797 Prospero, J. M.: Long-term measurements of the transport of African mineral dust to the southeastern United States:

798 Implications for regional air quality, *J. Geophys. Res. Atmos.*, 104(D13), 15917–15927,
799 doi:10.1029/1999JD900072, 1999.

800 Reid, J. S., Benedetti, A., Colarco, P. R. and Hansen, J. A.: International Operational Aerosol Observability
801 Workshop, *Bull. Am. Meteorol. Soc.*, 92(6), ES21-ES24, doi:10.1175/2010BAMS3183.1, 2010.

802 Reinfried, F., Tegen, I., Heinold, B., Hellmuth, O., Schepanski, K., Cubasch, U., Huebener, H. and Knippertz, P.:
803 Simulations of convectively-driven density currents in the Atlas region using a regional model: Impacts on
804 dust emission and sensitivity to horizontal resolution and convection schemes, *J. Geophys. Res. Atmos.*,
805 114(D8), doi:10.1029/2008JD010844, 2009.

806 Ridley, D. A., Heald, C. L., Pierce, J. R. and Evans, M. J.: Toward resolution-independent dust emissions in global
807 models: Impacts on the seasonal and spatial distribution of dust, *Geophys. Res. Lett.*, 40(11), 2873–2877,
808 doi:10.1002/grl.50409, 2013.

809 Roberts, A. J., Woodage, M. J., Marsham, J. H., Highwood, E. J., Ryder, C. L., McGinty, W., Wilson, S., and
810 Crook, J.: Can explicit convection improve modelled dust in summertime West Africa?, *Atmos. Chem.*
811 *Phys.*, 18, 9025-9048, <https://doi.org/10.5194/acp-18-9025-2018>, 2018.

812 Saleeby, S. M., van den Heever, S. C., Bukowski, J., Walker, A. L., Solbrig, J. E., Atwood, S. A., Bian, Q.,
813 Kreidenweis, S. M., Wang, Y., Wang, J. and Miller, S. D.: The Influence of Simulated Surface Dust
814 Lofting Erodible Fraction on Radiative Forcing, *Atmos. Chem. Phys. Discuss.*, 2019, 1–35,
815 doi:10.5194/acp-2018-1302, 2019.

816 Schepanski, K., Knippertz, P., Fiedler, S., Timouk, F. and Demarty, J.: The sensitivity of nocturnal low-level jets
817 and near-surface winds over the Sahel to model resolution, initial conditions and boundary-layer set-up.
818 *Q.J.R. Meteorol. Soc.*, 141, 1442-1456. doi:10.1002/qj.2453, 2015.

819 Seigel, R. B. and van den Heever, S. C.: Dust Lofting and Ingestion by Supercell Storms, *J. Atmos. Sci.*, 69(5),
820 1453–1473, doi:10.1175/JAS-D-11-0222.1, 2012.

821 Sessions, W. R., Reid, J. S., Benedetti, A., Colarco, P. R., da Silva, A., Lu, S., Sekiyama, T., Tanaka, T. Y.,
822 Baldasano, J. M., Basart, S., Brooks, M. E., Eck, T. F., Iredell, M., Hansen, J. A., Jorba, O. C., Juang, H.-
823 M. H., Lynch, P., Morcrette, J.-J., Moorthi, S., Mulcahy, J., Pradhan, Y., Razinger, M., Sampson, C. B.,
824 Wang, J. and Westphal, D. L.: Development towards a global operational aerosol consensus: basic
825 climatological characteristics of the International Cooperative for Aerosol Prediction Multi-Model
826 Ensemble (ICAP-MME), *Atmos. Chem. Phys.*, 15(1), 335–362, doi:10.5194/acp-15-335-2015, 2015.

827 Shwehdi, M. H.: Thunderstorm distribution and frequency in Saudi Arabia, *J. Geophys. Eng.*, 2(3), 252–267,
828 doi:10.1088/1742-2132/2/3/009, 2005.

829 Skamarock, W. C., Klemp, J. B., Dudhia, J. O. G. D., and Barker, D. M.: A description of the Advanced Research
830 WRF version 3, NCAR Tech. Note NCAR/TN-4751STR, NCAR, <http://dx.doi.org/10.5065/D68S4MVH>,
831 Boulder, CO, 2008.

832 Slingo, A., Ackerman, T. P., Allan, R. P., Kassianov, E. I., McFarlane, S. A., Robinson, G. J., Barnard, J. C., Miller,

833 M. A., Harries, J. E., Russell, J. E. and Dewitte, S.: Observations of the impact of a major Saharan dust
834 storm on the atmospheric radiation balance, *Geophys. Res. Lett.*, 33(24), doi:10.1029/2006GL027869,
835 2006.

836 Sokolik, I. N. and Toon, O. B.: Direct radiative forcing by anthropogenic airborne mineral aerosols, *Nature*,
837 381(6584), 681–683, doi:10.1038/381681a0, 1996.

838 Stafoggia, M., Zauli-Sajani, S., Pey, J., Samoli, E., Alessandrini, E., Basagaña, X., Cernigliaro, A., Chiusolo, M.,
839 Demaria, M., Díaz, J., Faustini, A., Katsouyanni, K., Kelessis, A. G., Linares, C., Marchesi, S., Medina, S.,
840 Pandolfi, P., Pérez, N., Querol, X., Randi, G., Ranzi, A., Tobias, A., Forastiere, F. and null null: Desert
841 Dust Outbreaks in Southern Europe: Contribution to Daily PM₁₀ Concentrations and Short-Term
842 Associations with Mortality and Hospital Admissions, *Environ. Health Perspect.*, 124(4), 413–419,
843 doi:10.1289/ehp.1409164, 2016.

844 Stephens, G. L., L'Ecuyer, T., Forbes, R., Gettelmen, A., Golaz, J.-C., Bodas-Salcedo, A., Suzuki, K., Gabriel, P.,
845 and Haynes, J.: Dreary state of precipitation in global models, *J. Geophys. Res.*, 115, D24211,
846 doi:[10.1029/2010JD014532](https://doi.org/10.1029/2010JD014532), 2010.

847 Sun, Y., Solomon, S., Dai, A., and Portmann, R. W.: How often does it rain? *J. Clim.*, 19, 916–934,
848 doi:[10.1175/JCLI3672.1](https://doi.org/10.1175/JCLI3672.1), 2006.

849 Takemi, T.: Importance of the Numerical Representation of Shallow and Deep Convection for Simulations of
850 Dust Transport over a Desert Region, *Adv. Meteorol.*, vol. 2012, 1-13, doi: 10.1155/2012/413584, 2012.

851 Tanaka, T. Y. and Chiba, M.: A numerical study of the contributions of dust source regions to the global dust
852 budget, *Glob. Planet. Change*, 52(1–4), 88–104, doi:10.1016/J.GLOPLACHA.2006.02.002, 2006.

853 Tegen, I. and Lacis, A. A.: Modeling of particle size distribution and its influence on the radiative properties of
854 mineral dust aerosol, *J. Geophys. Res. Atmos.*, 101(D14), 19237–19244, doi:10.1029/95JD03610, 1996.

855 Teixeira, J. C., Carvalho, A. C., Tuccella, P., Curci, G. and Rocha, A.: WRF-chem sensitivity to vertical resolution
856 during a saharan dust event, *Phys. Chem. Earth, Parts A/B/C*, 94, 188–195,
857 doi:10.1016/J.PCE.2015.04.002, 2016.

858 Todd, M. C., Bou Karam, D., Cavazos, C., Bouet, C., Heinold, B., Baldasano, J. M., Cautenet, G., Koren, I., Perez,
859 C., Solmon, F., Tegen, I., Tulet, P., Washington, R. and Zakey, A.: Quantifying uncertainty in estimates of
860 mineral dust flux: An intercomparison of model performance over the Bodélé Depression, northern Chad, *J.*
861 *Geophys. Res. Atmos.*, 113(D24), doi:10.1029/2008JD010476, 2008.

862 Tulet, P., Crahan-Kaku, K., Leriche, M., Aouizerats, B. and Crumeyrolle, S.: Mixing of dust aerosols into a
863 mesoscale convective system: Generation, filtering and possible feedbacks on ice anvils, *Atmos. Res.*,
864 96(2–3), 302–314, doi:10.1016/J.ATMOSRES.2009.09.011, 2010.

865 Twohy, C. H., Kreidenweis, S. M., Eidhammer, T., Browell, E. V., Heymsfield, A. J., Bansemer, A. R., Anderson, B.
866 E., Chen, G., Ismail, S., DeMott, P. J. and Van Den Heever, S. C.: Saharan dust particles nucleate droplets
867 in eastern Atlantic clouds, *Geophys. Res. Lett.*, 36(1), doi:10.1029/2008GL035846, 2009.

868 Uno, I., Wang, Z., Chiba, M., Chun, Y. S., Gong, S. L., Hara, Y., Jung, E., Lee, S.-S., Liu, M., Mikami, M., Music,

869 S., Nickovic, S., Satake, S., Shao, Y., Song, Z., Sugimoto, N., Tanaka, T. and Westphal, D. L.: Dust model
870 intercomparison (DMIP) study over Asia: Overview, *J. Geophys. Res. Atmos.*, 111(D12),
871 doi:10.1029/2005JD006575, 2006.

872 van Donkelaar, A., Martin, R. V, Brauer, M., Kahn, R., Levy, R., Verduzco, C. and Villeneuve, P. J.: Global
873 estimates of ambient fine particulate matter concentrations from satellite-based aerosol optical depth:
874 development and application, *Environ. Health Perspect.*, 118(6), 847–855, doi:10.1289/ehp.0901623, 2010.

875 Woodage, M. J. and Woodward, S.: U.K. HiGEM: Impacts of Desert Dust Radiative Forcing in a High-Resolution
876 Atmospheric GCM, *J. Clim.*, 27(15), 5907–5928, doi:10.1175/JCLI-D-13-00556.1, 2014.

877 Yang, Q., Easter, R. C., Campuzano-Jost, P., Jimenez, J. L., Fast, J. D., Ghan, S. J., Wang, H., Berg, L. K., Barth,
878 M. C., Liu, Y., Shrivastava, M. B., Singh, B., Morrison, H., Fan, J., Ziegler, C. L., Bela, M., Apel, E.,
879 Diskin, G. S., Mikoviny, T. and Wisthaler, A.: Aerosol transport and wet scavenging in deep convective
880 clouds: A case study and model evaluation using a multiple passive tracer analysis approach, *J. Geophys.*
881 *Res. Atmos.*, 120(16), 8448–8468, doi:10.1002/2015JD023647, 2015.

882 Yang, Z.-L., Niu, G.-Y., Mitchell, K. E., Chen, F., Ek, M. B., Barlage, M., Longuevergne, L., Manning, K., Niyogi,
883 D., Tewari, M. and Xia, Y.: The community Noah land surface model with multiparameterization options
884 (Noah-MP): 2. Evaluation over global river basins, *J. Geophys. Res. Atmos.*, 116(D12),
885 doi:10.1029/2010JD015140, 2011.

886 Yin, Y., Chen, Q., Jin, L., Chen, B., Zhu, S. and Zhang, X.: The effects of deep convection on the concentration and
887 size distribution of aerosol particles within the upper troposphere: A case study, *J. Geophys. Res. Atmos.*,
888 117(D22), doi:10.1029/2012JD017827, 2012.

889 Yu, Y., Notaro, M., Kalashnikova, O. V and Garay, M. J.: Climatology of summer Shamal wind in the Middle East,
890 *J. Geophys. Res. Atmos.*, 121(1), 289–305, doi:10.1002/2015JD024063, 2016.

891 Yuter, S. E. and Houze, R. A.: Three-Dimensional Kinematic and Microphysical Evolution of Florida
892 Cumulonimbus. Part II: Frequency Distributions of Vertical Velocity, Reflectivity, and Differential
893 Reflectivity, *Mon. Weather Rev.*, 123(7), 1941–1963, doi:10.1175/1520-
894 0493(1995)123<1941:TDKAME>2.0.CO;2, 1995.

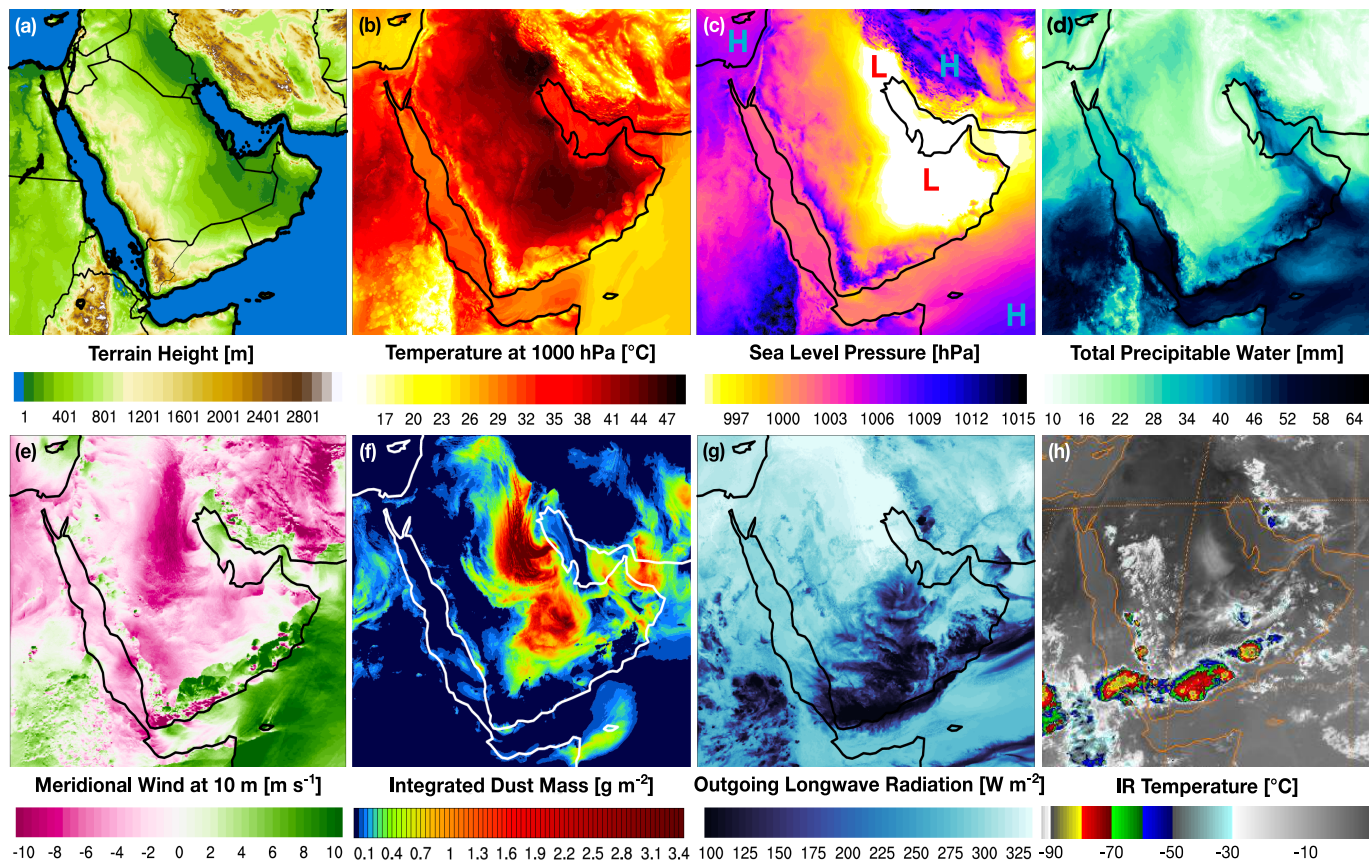
895 Zender, C. S., Miller, R. L. R. L. and Tegen, I.: Quantifying mineral dust mass budgets: Terminology, constraints,
896 and current estimates, *Eos, Trans. Am. Geophys. Union*, 85(48), 509–512, doi:10.1029/2004EO480002,
897 2004.

898 Zhao, C., Liu, X., Leung, L. R., Johnson, B., McFarlane, S. A., Gustafson Jr., W. I., Fast, J. D. and Easter, R.: The
899 spatial distribution of mineral dust and its shortwave radiative forcing over North Africa: modeling
900 sensitivities to dust emissions and aerosol size treatments, *Atmos. Chem. Phys.*, 10(18), 8821–8838,
901 doi:10.5194/acp-10-8821-2010, 2010.

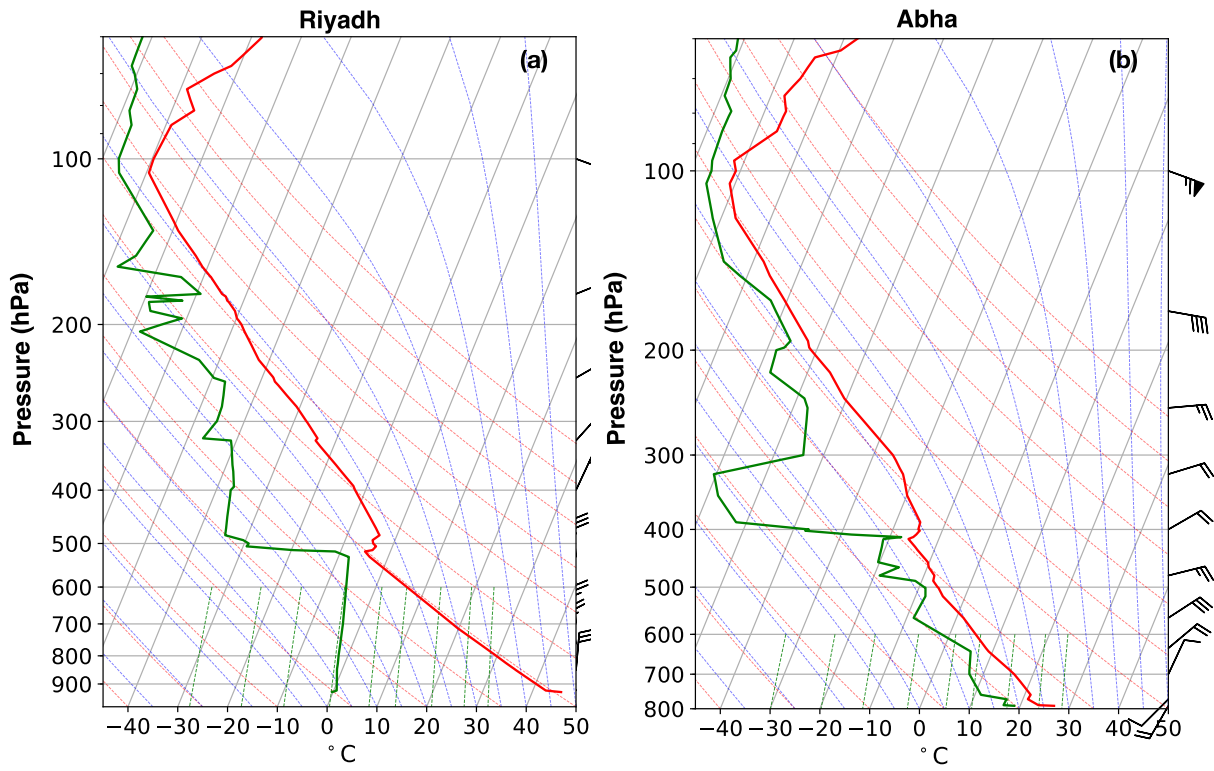
902

WRF-Chem Version 3.9.1.1	Parameterization / Model Option
Simulation Start	02-Aug-2016-00:00:00 UTC
Simulation End	05-Aug-2016-00:00:00 UTC
Domains	dx = dy = 45km / 15km / 3km
Nesting	One-way
Vertical Levels	50 stretched
Initialization	GDAS-FNL Reanalysis
Aerosol Module / Erodible Grid Map	GOCART / Ginoux et al. (2004)
Microphysics	Morrison 2-Moment
Radiation	RRTMG Longwave & Goddard Shortwave
Land Surface	Noah-MP Land Surface Model
Cumulus Schemes (45 km and 15 km grids only)	Betts–Miller–Janjic (BMJ) Kain–Fritsch (KF) Grell 3D Ensemble (GD) Tiedtke Scheme (TD) Simplified Arakawa–Schubert (AS)
Boundary Layer / Surface Layer	MYNN Level 3

903 **Table 1: Summary of WRF-Chem model options utilized and the simulation setup.**



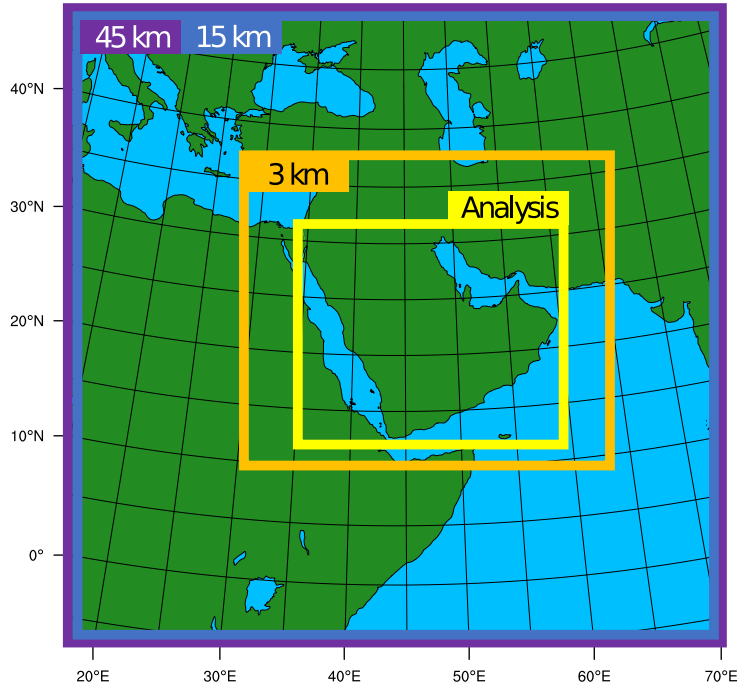
904
 905 **Figure 1: Case study topography and meteorology for August 3, 2016 at 15:00 UTC: (a) terrain height and national**
 906 **boundaries, (b) 1000 hPa Temperature, (c) sea level pressure, (d) total precipitable water, (e) meridional winds at 10 m**
 907 **AGL, (f) vertically integrated dust mass, (g) outgoing longwave radiation, and (h) IR temperature. Panel (h) is observed**
 908 **from Meteosat-7 while panels (a-g) are snapshots from the 3 km WRF-Chem simulation**



909

910 **Figure 2. Skew-T diagrams for two radiosonde release sites in Saudi Arabia on August 3, 2016 at 12:00 UTC for an inland**
 911 **location (a) and a location nearer to the coast (b).**

912



913

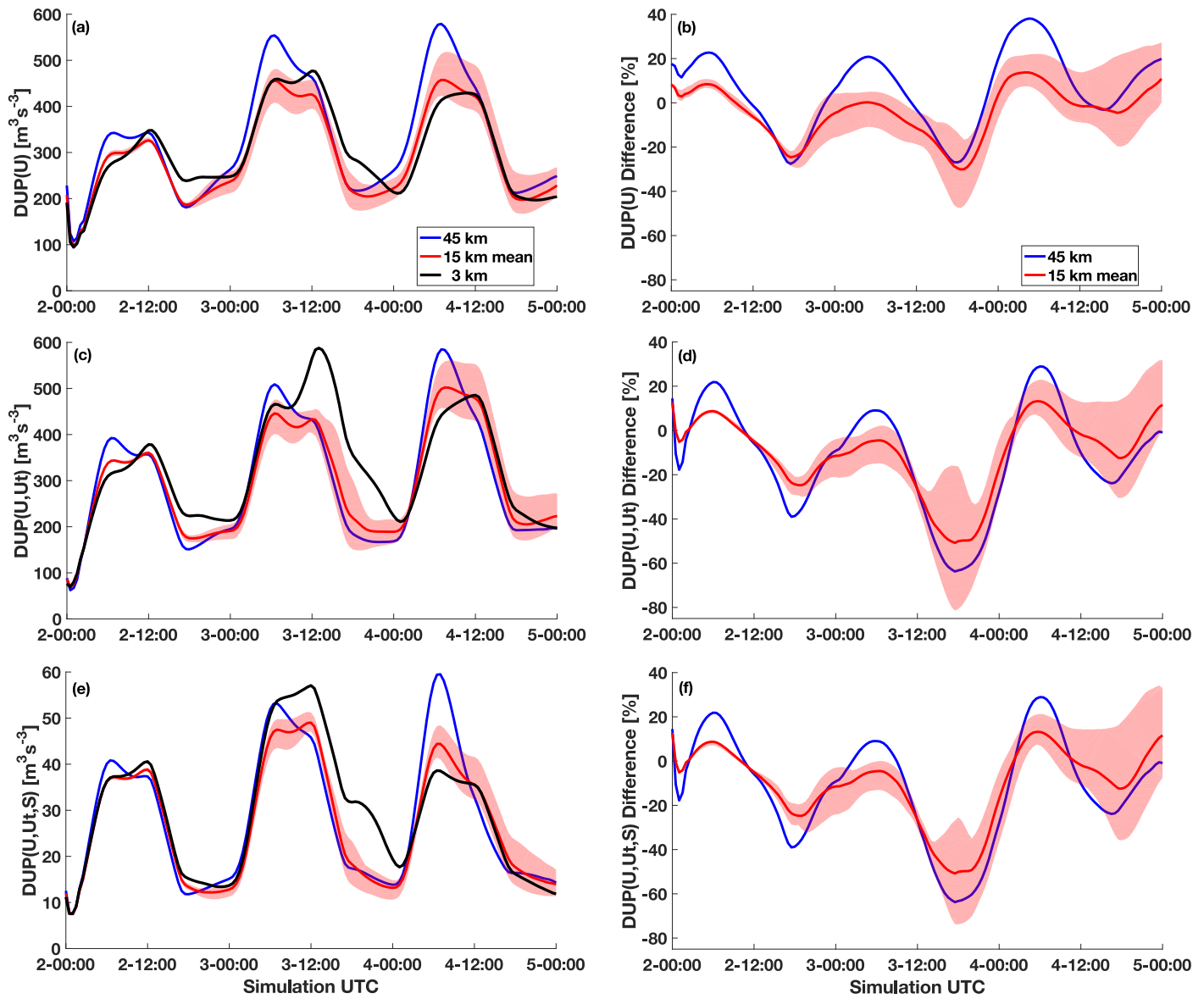
914

Figure 3: Model domain setup and analysis region for the 45 km (purple) and 15 km (blue) independent simulations with cumulus parameterizations, and the 3 km nested convection permitting simulation (orange). The averaging region for the

915

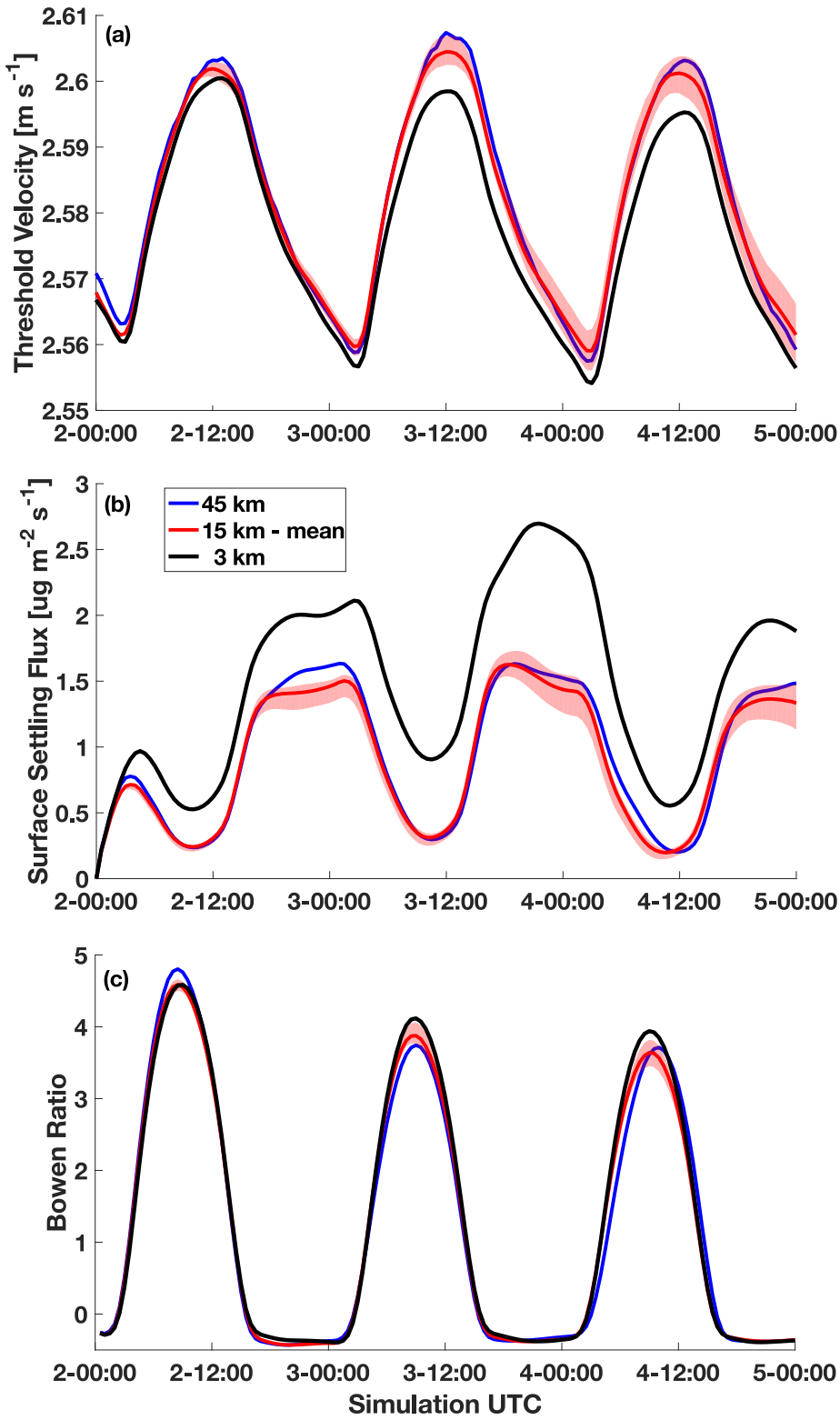
916

analysis is denoted in yellow.



917

918 **Figure 4: Left column: spatially averaged dust uplift potential for (a) $DUP(U)$, (c) $DUP(U,U_t)$, and (e) $DUP(U,U_t,S)$ for the**
 919 **45 km (blue), 15 km mean (red), and 3 km (black) simulations with the maximum and minimum spread across the 15 km**
 920 **simulations indicated in light red shading. Note that in panel (e) there is a change in scale in the ordinate. Right column:**
 921 **percent difference between the 3 km convection-permitting simulation and the simulations employing cumulus**
 922 **parameterizations for the different DUP parameters.**

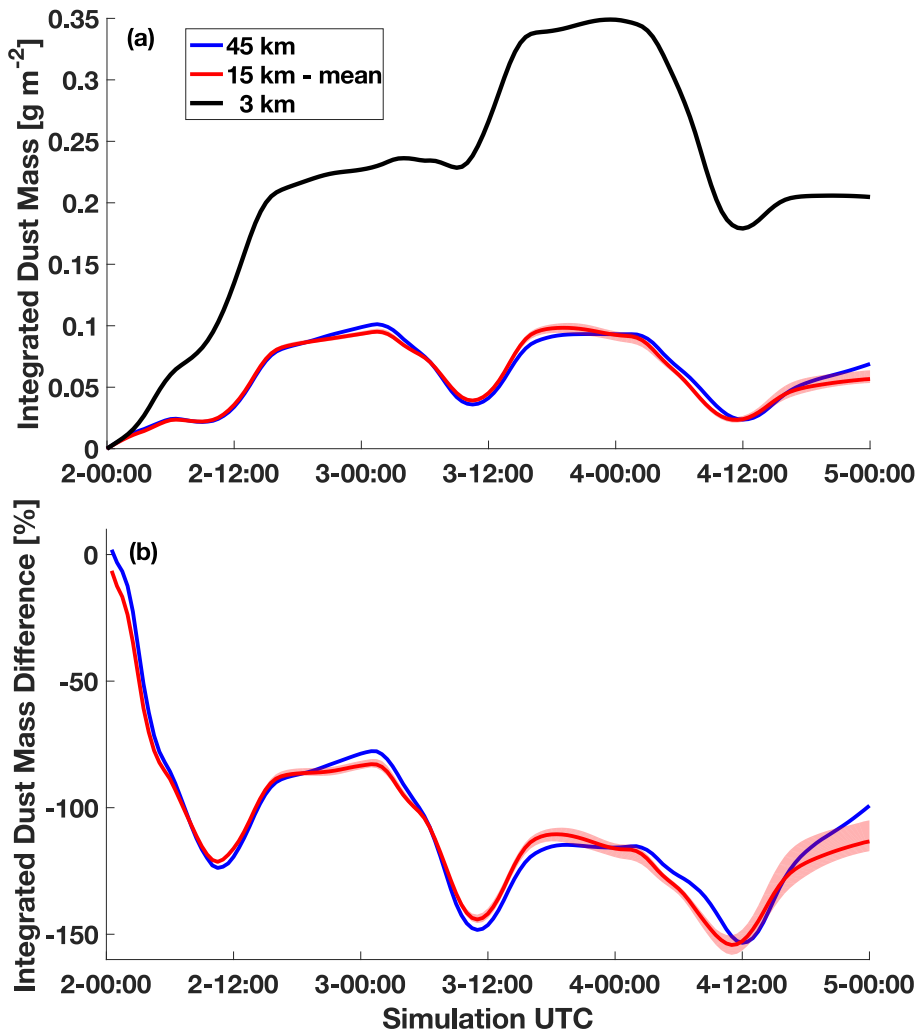


923

924

925

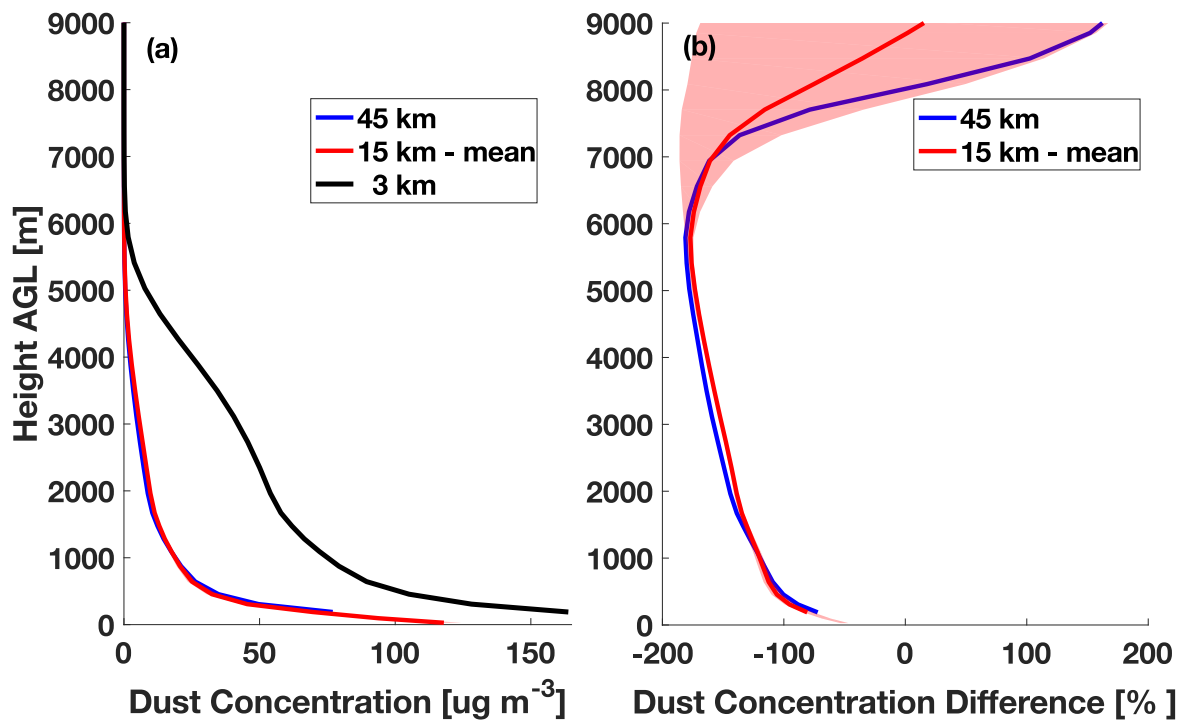
Figure 5: Spatially averaged (a) dust uplift threshold velocity, (b) dust surface settling flux, and (c) Bowen ratio of sensible to latent heat flux. Colors and shading are the same as in Fig. 4.



926

927

Figure 6: Spatially averaged, vertically integrated dust mass. Colors and shading are identical to that in previous figures.



928

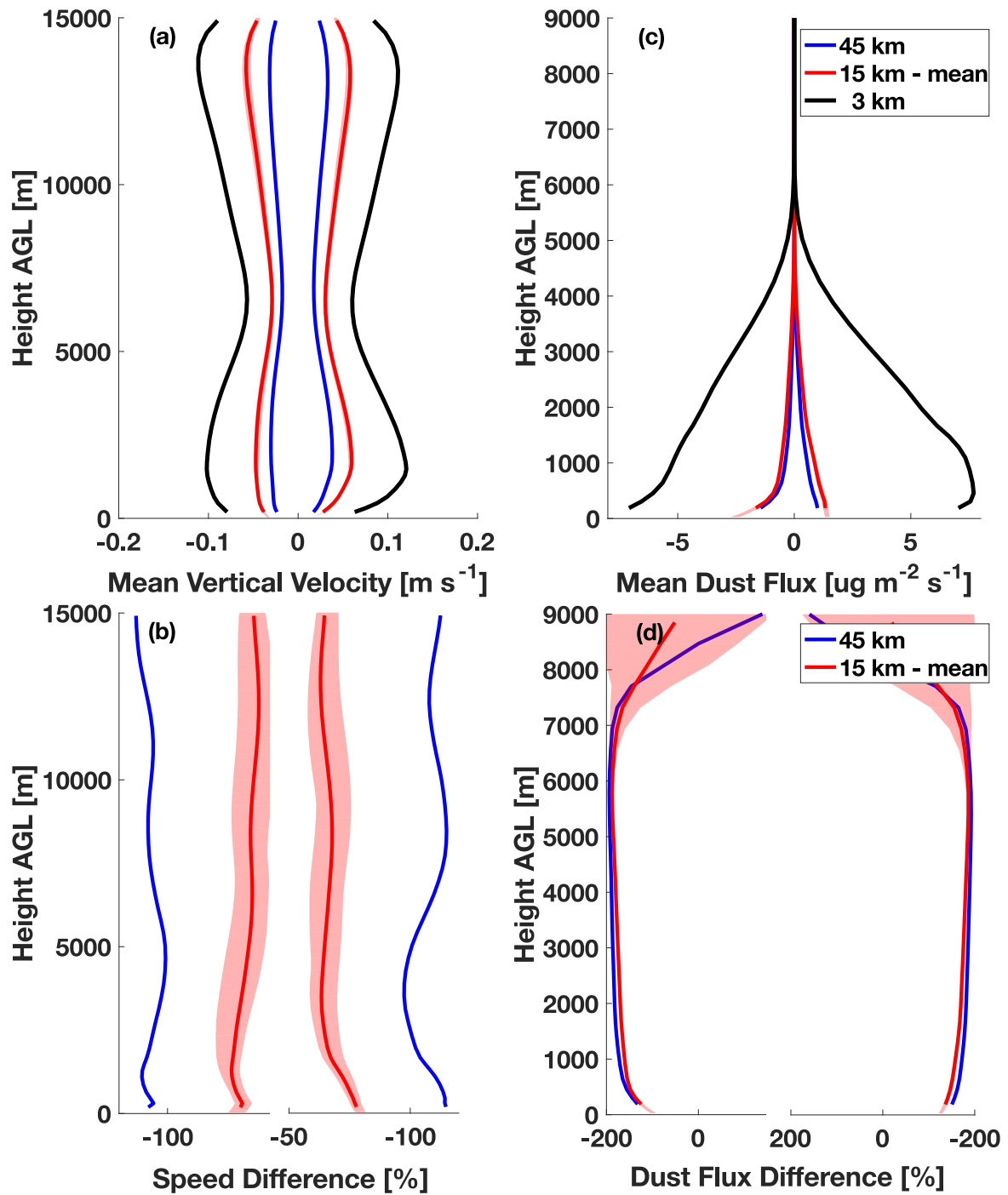
929

930

931

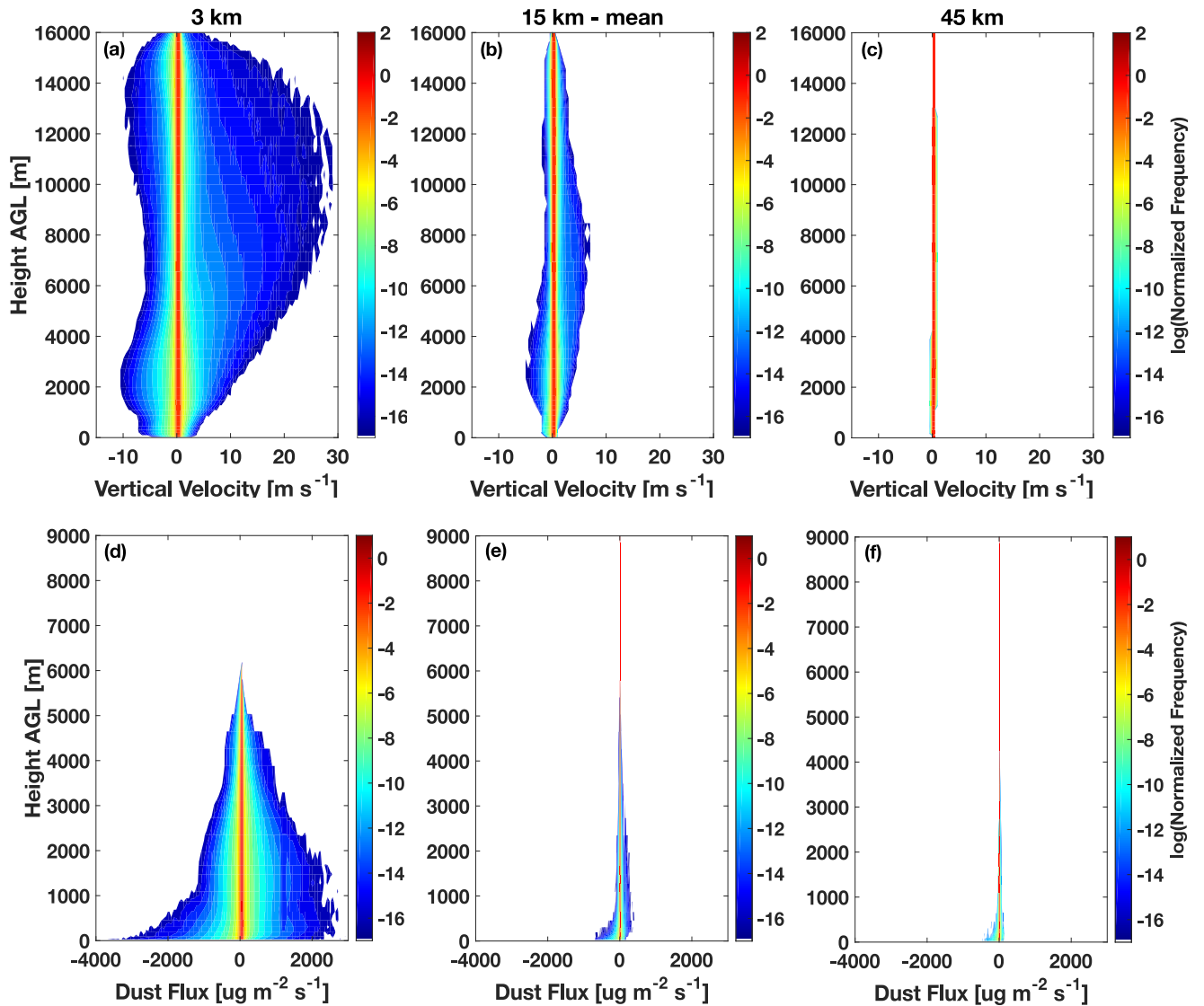
932

Figure 7: Spatially and time averaged vertical dust concentrations (a), with the (b) percent difference between the 3 km convection-permitting simulation and the simulations employing cumulus parameterizations. Plots are truncated at 9 km since the values above this height do not significantly vary from what is shown here. Colors and shading are identical to that in previous figures.



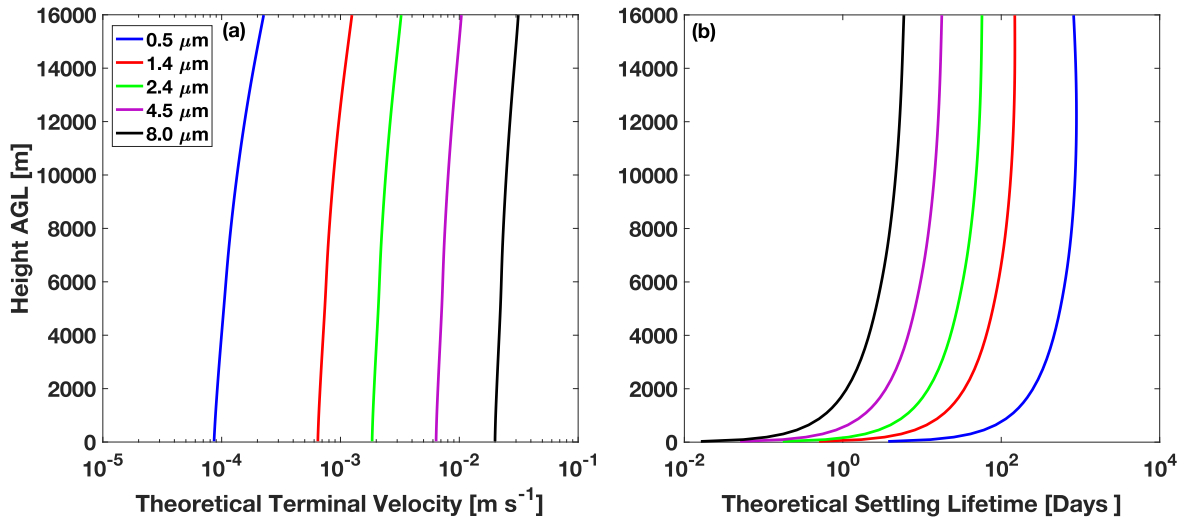
933

934 Figure 8. Left column: spatially and time averaged vertical velocities (a), with the (b) percent difference between the 3 km
 935 convection-permitting simulation and the simulations employing cumulus parameterizations. All velocities above or below
 936 zero were considered. Colors and shading are identical to that in previous figures. Right column: same but for vertical
 937 dust mass flux. Note that in panels (c) and (d) the vertical axes are truncated at 9 km since the values above this height do
 938 not significantly vary from what is shown here.



940

941 Figure 9: Top row: Contoured Frequency by Altitude Diagrams (CFADs) for vertical velocity, normalized by the number
 942 of grid points in each respective simulation. The contours are computed on a log scale to highlight the variances away
 943 from zero. Bottom row: same but for vertical dust mass flux. Note that the panels in the bottom row are truncated at 9
 944 km since the values above this height do not significantly vary from what is shown here.



945

946

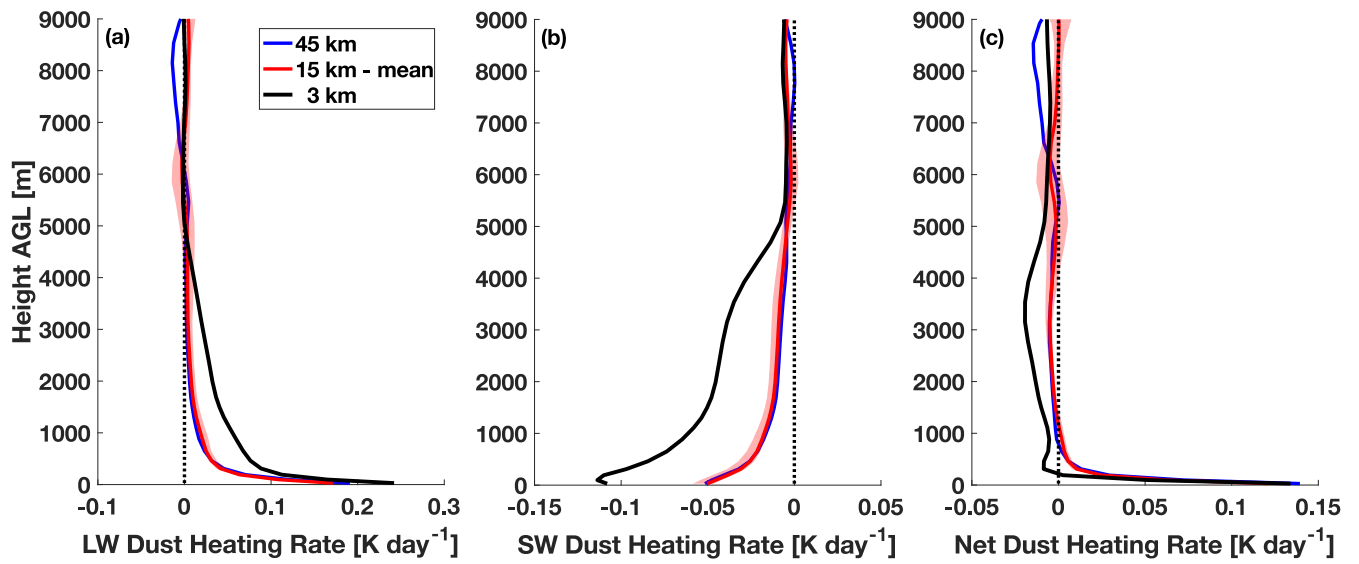
947

948

949

950

Figure 10: Theoretical terminal velocity of dust particles (a) based on Stokes settling velocity with slip correction for pressure dependence for the 5 effective radii of dust particles in WRF-Chem. The calculations assume no vertical motions, advection, deposition, coagulation, or condensation. (b) The lifetime of these theoretical dust particles based on their height in the atmosphere.



951

952

953

954

955

Figure 11: Spatially and time averaged longwave (a), shortwave (b), and net (c) dust heating rate profile for the 45 km (blue), 15 km mean (red), and 3 km (black) simulations with the maximum and minimum spread across the 15 km simulations indicated in light red shading. Plots are truncated at 9 km since the values above this height do not significantly vary from what is shown here.